bioRxiv preprint doi: https://doi.org/10.1101/2021.06.04.447058; this version posted June 4, 2021. The copyright holder for this preprint (which was not certified by peer review) is the author/funder, who has granted bioRxiv a license to display the preprint in perpetuity. It is made available under aCC-BY 4.0 International license.

System genetics in the rat HXB/BXH family identifies *Tti2* as a pleiotropic quantitative trait gene for adult hippocampal neurogenesis and serum glucose

Anna N. Grzyb[1, 2], Rupert W. Overall[1, 2], Jan Silhavy[3], Petr Mlejnek[3], Hana Malínská[4], Martina Hüttl[4], Irena Marková[4], Klaus S. Fabel[1, 2], Lu Lu[5], Ales Stuchlik[3], Robert W. Williams[5], Michal Pravenec[3], Gerd Kempermann[1, 2]*

[1] German Center for Neurodegenerative Diseases (DZNE) Dresden, Tatzberg 41, 01307 Dresden, Germany

[2] CRTD – Center for Regenerative Therapies Dresden, Technische Universität Dresden, Fetscherstraße 105, 01307 Dresden, Germany

[3] Institute of Physiology of the Czech Academy of Sciences, Videnska 1083, 14220 Prague 4, 142 20, Czech Republic

[4] Institute for Clinical and Experimental Medicine, Videnska 1958, 14021 Prague 4, 142 21, Czech Republic

[5] Department of Genetics, Genomics and Informatics, University of Tennessee Health Science Center, Memphis, TN 38163, USA

* Corresponding author

E-mail: gerd.kempermann@dzne.de or gerd.kempermann@tu-dresden.de

bioRxiv preprint doi: https://doi.org/10.1101/2021.06.04.447058; this version posted June 4, 2021. The copyright holder for this preprint (which was not certified by peer review) is the author/funder, who has granted bioRxiv a license to display the preprint in perpetuity. It is made available under a CC-BY 4.0 International license.

Abstract

Neurogenesis in the adult hippocampus contributes to learning and memory in the healthy brain but is dysregulated in metabolic and neurodegenerative diseases. The molecular relationships between neural stem cell activity, adult neurogenesis, and global metabolism are largely unknown. Here we applied unbiased systems genetic methods to quantify genetic covariation among adult neurogenesis and metabolic phenotypes in peripheral tissues of a genetically diverse family of rat strains, derived from a cross between the spontaneously hypertensive (SHR/OlaIpcv) strain and Brown Norway (BN-*Lx*/Cub). The HXB/BXH family is a very well established model to dissect genetic variants that modulate metabolic and cardiovascular disease and we have accumulated deep phenome and transcriptome data in a FAIR-compliant resource for systematic and integrative analyses. Here we measured rates of precursor cell proliferation, survival of new neurons, and gene expression in the hippocampus of the entire HXB/BXH family, including both parents. These data were combined with published metabolic phenotypes to detect a neurometabolic quantitative trait locus (QTL) for serum glucose and neuronal survival. We subsequently fine-mapped a key phenotype to a locus that includes the telo2-interacting protein 2 gene (*Tti2*)—a chaperone that modulates the activity and stability of PIKK kinases. To validate variants in or near *Tti2* as a cause for differences in neurogenesis and glucose levels, we generated a targeted frameshift mutation on the SHR/OlaIpcv background. Heterozygous SHR-*Tti2*$^{+/-}$ mutants had lower rates of hippocampal neurogenesis and hallmarks of dysglycemia compared to wild-type littermates. Our findings highlight *Tti2* as a causal genetic and molecular link between glucose metabolism and structural brain plasticity. In humans, more than 800 genomic variants are linked to *TTI2* expression, seven of which have associations to protein and blood stem cell factor concentrations, blood pressure and frontotemporal dementia.

bioRxiv preprint doi: https://doi.org/10.1101/2021.06.04.447058; this version posted June 4, 2021. The copyright holder for this preprint (which was not certified by peer review) is the author/funder, who has granted bioRxiv a license to display the preprint in perpetuity. It is made available under a CC-BY 4.0 International license.

Author summary

Metabolic and neurological disorders are often comorbid, suggesting that biological pathways which orchestrate peripheral homeostasis and the integrity of the nervous system intersect. The genetic architecture behind these relationships is still poorly described, in part because molecular processes in the human brain are very difficult to study. We thus used a rodent genetic reference population to investigate links between adult hippocampal neurogenesis—a cellular plasticity mechanism important for learning flexibility—and metabolism. We measured adult neurogenesis in the family of 30 HXB/BXH rat recombinant inbred strains, who are characterised by stable differences in metabolism, behaviour, and gene expression levels. Because gene variants affecting distinct traits segregated into different members of the family, we discovered that previously published phenotypes correlated to adult neurogenesis due to shared genomic sequence. We found that expression levels of *Tti2*—a part of a specialised protein chaperone complex regulating stability of PIKK kinases—were concomitantly influencing adult neurogenesis and serum glucose levels. In human populations hundreds of genomic variants regulate *TTI2* expression, potentially affecting brain function and glucose homeostasis.

bioRxiv preprint doi: https://doi.org/10.1101/2021.06.04.447058; this version posted June 4, 2021. The copyright holder for this preprint (which was not certified by peer review) is the author/funder, who has granted bioRxiv a license to display the preprint in perpetuity. It is made available under aCC-BY 4.0 International license.

Introduction

Epidemiological studies link components of the metabolic syndrome—a complex disorder characterised by the coexistence of obesity, insulin resistance, dyslipidaemia, and hypertension—to cognitive impairment and dementia [1]. Defective brain function is often seen as a consequence of longstanding metabolic deregulation. The full picture, however, is more complex. Several human phenome-wide association studies identified causal genetic loci that are shared between metabolic and neurological phenotypes [2–8], suggesting some degree of pleiotropy—a phenomenon whereby one gene variant affects multiple traits. Pleiotropy is widespread among model organisms [9–13] and humans [2,14–17] with an estimated median number of around six traits per locus [13]. Pleiotropic mutations can result in genetic covariance among phenotypes [10,12]. Cognition and metabolic homeostasis are both achieved through multiple elementary mechanisms at molecular, cellular, tissue, and inter-organ levels, some of which might be shared. To understand the biology underlying correlations between such complex functions, it is necessary to identify which exact processes are simultaneously affected by shared genetic variation.

Adult neurogenesis in the dentate gyrus (DG) of the hippocampus is required for cognitive flexibility of learning, efficient pattern separation and emotional processing in mammals [18], and thus embodies a functionally relevant and readily quantifiable parameter of hippocampal plasticity. In humans, according to the best available calculation, one third of dentate granule cells are born during adulthood [19]. The generation of new granule neurons in the DG is a complex multistep process, in the course of which neural precursor cell proliferation, as well as survival, maturation, and integration of newly born postmitotic cells are under the control of multiple genetic loci. Remarkably, cellular metabolism has been identified as a regulator of neural stem and progenitor cell maintenance, proliferation, and differentiation [20], yet the interactions of adult neurogenesis with systemic metabolism are far from being understood. Given the overall significance of metabolism for brain function in health and disease, there is

bioRxiv preprint doi: https://doi.org/10.1101/2021.06.04.447058; this version posted June 4, 2021. The copyright holder for this preprint (which was not certified by peer review) is the author/funder, who has granted bioRxiv a license to display the preprint in perpetuity. It is made available under a CC-BY 4.0 International license.

a high likelihood that direct causal links exist between structural brain plasticity and metabolic traits and states.

Natural genetic variation present in genetically diverse mouse populations contributes to up to ten-fold differences in the net production of new neurons [21,22]—values much larger than the induction achieved by environmental interventions within a single genetic background. This enormous genetic potential inherent in rodent strains can be utilised to dissect the molecular interaction networks not only underlying adult neurogenesis as such, but also its connections with homeostatic mechanisms in peripheral tissues.

We thus employed a family of 30 fully inbred recombinant HXB/BXH rat strains, which have been derived by reciprocal mating of a spontaneously hypertensive rat line (SHR/OlaIpcv, hereafter referred to as SHR) with the normotensive BN-*Lx*/Cub—a Brown Norway (BN) congenic rat with a mutation that causes a polydactyly-luxate phenotype [23,24]. Besides hypertension, SHR manifests other hallmarks of metabolic syndrome [25–27], as well as cognitive deficits [28,29], and brain morphological changes [30,31]. The HXB/BXH family were developed to map quantitative trait loci (QTL) for hypertension and morphological abnormalities associated with polydactyly-luxate syndrome [23,24], but they are of great utility for genetic mapping of a wider spectrum of phenotypes. The HXB/BXH family have become the most thoroughly characterised rat reference population within the Rat Hybrid Diversity Panel [32]. Over 200 metabolic, endocrinological, behavioural and developmental phenotypes, along with gene expression profiles in peripheral tissues, are publicly accessible in a FAIR-compliant format at the GeneNetwork database [33,34]. The stable genetic background of these recombinant inbred lines enables truly systemic integration of phenotypic and omics data [32]. Accordingly, the HXB/BXH family have been used to clone genes associated with several disease quantitative trait loci (QTL) and discover gene regulatory networks relevant for human diseases [26,27,35–41]. The family offer levels of genetic diversity comparable to human populations [42,43] and hence allow for the separation of phenotypes modulated by different sets of gene variants. Correlations between phenotypes, in turn, suggest shared genetic causality [10,44].

bioRxiv preprint doi: https://doi.org/10.1101/2021.06.04.447058; this version posted June 4, 2021. The copyright holder for this preprint (which was not certified by peer review) is the author/funder, who has granted bioRxiv a license to display the preprint in perpetuity. It is made available under a CC-BY 4.0 International license.

In the present study, we quantified adult hippocampal neurogenesis in all existing HXB/BXH family members and parents. We aimed to find out the extent of genetic correlations between neurogenesis and peripheral metabolism, and sought to identify common loci that cause these correlations. The data reported here were submitted into public databases as a part of the HXB/BXH phenome resource.

bioRxiv preprint doi: https://doi.org/10.1101/2021.06.04.447058; this version posted June 4, 2021. The copyright holder for this preprint (which was not certified by peer review) is the author/funder, who has granted bioRxiv a license to display the preprint in perpetuity. It is made available under a CC-BY 4.0 International license.

Results

Adult neurogenesis in HXB/BXH strains

We quantified adult hippocampal neurogenesis in DG of young male rats from all 30 HXB/BXH family members, as well as the parental founder strains BN and SHR. Numbers of proliferating stem and progenitor cells were estimated using immunohistochemistry against the Ki67 antigen (Fig. 1A, D). Dividing cells were also labelled with BrdU at 10 weeks of age and surviving progeny were quantified four weeks later (Fig. 1B, E), after which time point new cells are likely to persist for very long periods of time [45,46]. Newborn cells were identified as neurons by double labelling with neuronal marker, NeuN (Rbfox3, Fig. 1C). Among 3814 $BrdU^+$ cells in 38 individuals, we detected only a single $BrdU^+$/S100□$^+$ astrocyte. We conclude that either astrogliogenesis is negligible in the DG of young HXB/BXH rats, or S100□ (the standard marker in mice in this case) is not expressed in newly-born astrocytes in these lines. Notably, over 90 % of BrdU-positive cells were neurons (Fig. 1F). Hence, we used the numbers of surviving BrdU-positive cells as an approximation of net neurogenesis within the HXB/BXH family. The majority of dividing cells in the DG are transient amplifying progenitors, which remain tightly clustered together (Fig. 1A–A''). We quantified the number of such clusters of proliferating cells, assuming that each cluster arises from an activated stem cell. The number of clusters tightly correlated to counts of individual cells (Pearson's r^2 = 0.92; Fig. 1G). Such high correlation suggested that the numbers of proliferating cells were determined by the numbers of activated stem cells rather than differences in lineage progression or cell cycle dynamics in these animals, and pointed to a stereotyped pattern of lineage progression.

Fig. 1. Adult neurogenesis in the HXB/BXH family.

(A) Proliferating precursor cells were stained for Ki67, a marker of actively cycling cells. (A'-A'') Proliferating cells occur in tightly packed clusters, which are likely to arise from single activated stem cells. (A') High power view of two clusters indicated by arrows in (A). (A'') An

bioRxiv preprint doi: https://doi.org/10.1101/2021.06.04.447058; this version posted June 4, 2021. The copyright holder for this preprint (which was not certified by peer review) is the author/funder, who has granted bioRxiv a license to display the preprint in perpetuity. It is made available under a CC-BY 4.0 International license.

example of a single large cluster of Ki67⁺ cells. (B) New cells in the DG were identified by DAB-immunostaining for BrdU 4 weeks after the last BrdU injection. (B') High power view of cells indicated by an arrow. (C) BrdU-positive cells (magenta, arrowhead) were identified as neurons by confocal microscopy after co-labelling with a neuronal marker, NeuN (green). (D-E) The number of proliferating (D) and surviving (E) cells in the DG of HXB/BXH, BN (red) and SHR (blue) strains. (F) Distribution of neuronal percentages among newborn cells across HXB/BXH family confirms that more than 90% of newborn cells are neurons. Box and whisker plot: centre line - median; upper and lower hinges - first and third quartiles; whiskers - highest and lowest values within 1.5 times the interquartile range outside hinges; dots - outlying data points. (G) Correlation between number of clusters and individual counts of proliferating cells. (H-I) Quantile-quantile plots of neurogenesis traits indicate normal distribution of strain means. (J) Rates of precursor cell proliferation are not predicting the number of surviving cells. *r*, Pearson's product-moment correlation coefficient. Scale bar, 100 and 20 μm in A and B, 20 μm in A', A'', B'' and C.

Proliferation and survival differed between 2- and 3-fold across the strains (Fig. 1D, E) and were normally distributed (Fig. 1H, I; BrdU: $W = 0.983$, $p = 0.88$; Ki67: $W = 0.976$, $p = 0.67$; Shapiro-Wilk test), consistent with the multigenic regulation of adult neurogenesis. Transgressive segregation was observed for both traits, indicating that genes with positive effect on neurogenesis were distributed between parents. The heritability was estimated as 0.41 and 0.29 for survival and proliferation, respectively. Interestingly, proliferation levels did not predict the rates of survival, as these measures did not correlated to each other ($r^2 = 0.026$; Fig. 1J). This finding implies that, under standard laboratory conditions, these two aspects of neurogenesis are influenced by largely separate sets of genes.

bioRxiv preprint doi: https://doi.org/10.1101/2021.06.04.447058; this version posted June 4, 2021. The copyright holder for this preprint (which was not certified by peer review) is the author/funder, who has granted bioRxiv a license to display the preprint in perpetuity. It is made available under a CC-BY 4.0 International license.

Shared QTL for neurogenesis and serum glucose

The search for genetic associations between adult neurogenesis and physiological traits was performed in several steps. First, we identified QTL for both neurogenic traits (Fig. 2A, B). We detected a suggestive QTL for net neurogenesis on chromosome 16 (LOD = 3.12, genome-wide corrected *p* value = 0.14) and a weak suggestive QTL for proliferation on chromosome 17 (LOD = 2.39, *p* = 0.52). Second, we identified phenotypes from the GeneNetwork database [34] that significantly correlated to both traits (Table 1). We then used these phenotypes as covariates in conditional QTL scans to screen for potential interactions at a genomic level. A substantial change in the LOD score after using another phenotype as a covariate indicates that genetic variation within a QTL may have pleiotropic effects on these two phenotypes [47]. Among pairs of correlating phenotypes, we detected only one such association: QTL mapping for net neurogenesis revealed a LOD drop below suggestive level to 0.43 after conditioning on serum glucose levels. Accordingly, an overlapping significant QTL for serum glucose was found on chromosome 16 (LOD = 5.13, *p* = 0.0065; Fig. 2C). This locus explained 37 % of the genetic variance in adult neurogenesis and 61 % of the genetic variance in serum glucose. The SHR allele was associated with an average decrease in BrdU cell numbers by 584 and in serum glucose by 0.656 mmol/L.

bioRxiv preprint doi: https://doi.org/10.1101/2021.06.04.447058; this version posted June 4, 2021. The copyright holder for this preprint (which was not certified by peer review) is the author/funder, who has granted bioRxiv a license to display the preprint in perpetuity. It is made available under aCC-BY 4.0 International license.

Table 1. Published phenotypes correlating to adult neurogenesis in HXB/BXH family.

Phenotype	*r*	N	*p*-value	ID
Net neurogenesis (BrdU$^+$ cells)				
Glucose concentrations	0.57	24	0.0031	10003
Serum triglyceride concentrations	0.46	24	0.023	10014
Liver triglycerides	0.41	29	0.026	10119
Relative kidney weight	-0.40	28	0.034	10025
Serum chromogranin A levels	0.37	30	0.043	10132
Proliferation (Ki67$^+$ cells)				
Adrenal phenyletanolamine-N-mythyltransferase	0.58	30	0.0006	10151
Adrenal dopamine	0.52	30	0.0031	10106
Adrenal epinephrine	0.47	30	0.0081	10105
Relative kidney weight	-0.45	28	0.015	10025
Insulin stimulated lipogenesis in epididymal fat	-0.44	31	0.012	10148
Adrenal chromogranin A levels	0.43	30	0.016	10133
Serum corticosterone levels after immobilization stress	-0.42	23	0.043	10064
Serum triglyceride concentrations, fed high fructose diet for 2 weeks	0.42	24	0.039	10016
Adrenal norepinephrine	0.40	30	0.029	10107
Urine calcium	0.39	28	0.041	10179
Basal lipogenesis in epididymal fat	-0.38	31	0.033	10146

All phenotypes were measured in male rats aged between 6 to 10 weeks. Details can be found in the GeneNetwork database (www.genenetwork.org). *r*, Pearson's product correlation coefficient; N, number of overlapping strains; ID, GeneNetwork identifier.

Fig. 2. *Tti2* is a candidate gene for common net neurogenesis and serum glucose quantitative trait locus (QTL).

(A-E) Whole-genome quantitative trait locus mapping for indicated traits. The genome-wide significant ($p < 0.05$) and suggestive ($p < 0.63$) thresholds of the logarithm of the odds (LOD) score (green and grey horizontal dashed lines, respectively) were calculated using permutations and corrected *p*-values are shown adjacent to the highest association in (A-C). QTL for net adult neurogenesis and a positively correlating phenotype, serum glucose level, have an overlapping pattern on chromosome 16. (D) An eigenvector of the two phenotypes (an *eigenphenotype*–the first principal component) was used to calculate a common confidence interval for the shared QTL (shaded areas in D and E). (E) *Tti2* gene, whose

bioRxiv preprint doi: https://doi.org/10.1101/2021.06.04.447058; this version posted June 4, 2021. The copyright holder for this preprint (which was not certified by peer review) is the author/funder, who has granted bioRxiv a license to display the preprint in perpetuity. It is made available under a CC-BY 4.0 International license.

genomic position is indicated by an orange triangle, has a local expression QTL within the eigenphenotype QTL confidence interval on chromosome 16 in all tested tissues. For clarity, in (D) and (E) only fragments of the chromosome 16 were plotted. (F) *Tti2* expression in the hippocampus or tissues relevant for regulation of glucose homeostasis, as indicated in the figure, is correlated to net neurogenesis and serum glucose. Colour specifies parental genotypes at the marker, which had the highest LOD score association with the eigenphenotype.

Finally, to derive a confidence interval for the joint survival-serum glucose QTL, we combined the variance from both traits using their first principal component, here referred to as an eigenphenotype. (Fig. 2D). The eigenphenotype QTL (LOD = 4.62, p = 0.014) spanned 4.2 Mb from genomic position 62.1 to 66.3 Mb and contained 11 protein-coding and 4 non-coding RNA genes.

Tti2 **is a candidate quantitative trait gene**

Genetic correlations between phenotypes can result from variation in shared regulatory genes or from linkage disequilibrium. In linkage disequilibrium, distinct genes governing each phenotype co-segregate together in the limited population of recombinant strains due to their physical proximity in the genome. To distinguish these scenarios and prioritise candidate genes for each phenotype, we used transcriptional profiles in tissues relevant for adult neurogenesis and metabolic regulation to cross-correlate with phenotypes and genetic markers. To that end, we profiled gene expression data from hippocampi of HXB/BXH and parental strains using microarrays. We also used published gene expression data sets from the soleus muscle, liver, perirenal fat, kidney, adrenal gland, left ventricle and aorta. Expression of only one single gene, Telo2-interacting protein 2 (*Tti2*), correlated significantly to both traits across all data sets (Fig. 2F). *Tti2* mRNA expression was linked to multi-tissue cis-eQTL mapped within the neurogenesis-glucose QTL on chromosome 16 (Fig. 2E). We thus carried out conditional mapping for neurogenesis and serum glucose using expression of *Tti2* as a covariate. Substantial drop in the LOD score between unconditioned and

bioRxiv preprint doi: https://doi.org/10.1101/2021.06.04.447058; this version posted June 4, 2021. The copyright holder for this preprint (which was not certified by peer review) is the author/funder, who has granted bioRxiv a license to display the preprint in perpetuity. It is made available under a CC-BY 4.0 International license.

234 conditioned scans strongly suggests that the QTL effect is mediated by the gene
235 expression—consistent with the flow of causation from genes to phenotypes [47–49]. Using
236 *Tti2* expression in the hippocampus as a covariate decreased the LOD score for adult
237 neurogenesis by 2.34 (LOD = 0.78). To investigate the effect of *Tti2* expression in peripheral
238 tissues on serum glucose mapping, we first summarised *Tti2* expression levels in these data
239 sets as an eigengene (the first principal component). Using the *Tti2* eigengene as a covariate
240 in QTL mapping decreased the LOD score for serum glucose by 2.76 (LOD = 2.37). The
241 conditional LOD values for both phenotypes were below suggestive level. The SHR allele
242 was associated with higher levels of *Tti2* mRNA, which we verified using quantitative RT-
243 PCR in RNA isolated from the hippocampus, liver, muscle, kidney and pancreas (Table S1).
244 The allelic variation underlying a QTL can either change the expression level of a gene, or
245 the function of its product by altering its structure. We inspected the genes located within the
246 eigenphenotype QTL confidence interval for non-synonymous amino acid substitutions.
247 Interestingly, only *Tti2* carried several missense mutations, including one at a highly
248 conserved position, although none of the substitutions were predicted as damaging by
249 Polyphen or SIFT (Table S2). Together, these data support *Tti2* as a causal candidate gene
250 for the combined serum glucose and net neurogenesis QTL.

251 **Reduced *Tti2* expression impairs adult neurogenesis and metabolic homeostasis**

252 To evaluate whether expression of *Tti2* might be indeed causally linked to regulation of
253 net adult neurogenesis and serum glucose, we derived heterozygous *Tti2* knockout rats on
254 the SHR background. Using zinc finger nuclease, we introduced an 8-bp deletion in the first
255 exon of *Tti2*, which resulted in a frameshift mutation, presumably generating a non-functional
256 protein. Heterozygous male rats were compared to wild type littermates to assess
257 consequences of the reduction of available Tti2 for adult hippocampal neurogenesis and
258 metabolism.
259 Net adult neurogenesis decreased by 21 % in the DG of 3-month-old SHR-*Tti2*$^{+/-}$
260 compared to their wild-type SHR littermates (Fig. 3A; see Table 2 for detailed statistical

bioRxiv preprint doi: https://doi.org/10.1101/2021.06.04.447058; this version posted June 4, 2021. The copyright holder for this preprint (which was not certified by peer review) is the author/funder, who has granted bioRxiv a license to display the preprint in perpetuity. It is made available under aCC-BY 4.0 International license.

analysis). Concomitantly, heterozygous animals exhibited extensive alterations in metabolic parameters (Fig. 3; Fig. S1; Table 2 and 3). Heterozygous knock-out of *Tti2* resulted in lower plasma glucose and insulin levels (Fig. 3B-C). SHR-*Tti2*$^{+/-}$ rats had also elevated plasma triglycerides (TG; Fig. 3D) and non-esterified fatty acids (NEFA; Fig. 3F) compared to SHR control. Changes in plasma lipid profile were accompanied by decrease of liver TG and cholesterol content (Fig. 3G-H). However, we did not observe an effect on total or HDL-bound fraction of plasma cholesterol (Fig. 3E, Fig. S1H). In SHR-*Tti2*$^{+/-}$ animals we observed changes in body composition and organ sizes, including lipogenic tissues: they had smaller livers and epididymal fat deposits and increased perirenal fat weights (Fig. S1B-D). On the other hand, knock-out of Tti2 did not affect the weight of brown adipose tissue (BAT; Fig. S1E). While the heterozygous rats were slightly larger compared to the control animals (Fig. S1A), this difference was not statistically significant.

Fig. 3. Knock-down of Tti2 leads to decreased hippocampal neurogenesis and impaired glucose homeostasis.

(A-H) Three-months old heterozygous SHR-*Tti2*$^{+/-}$ rats and wild type SHR-*Tti2*$^{+/+}$ littermates (denoted as SHR) were assessed for the phenotypes indicated in the figure. (I-K) Glucose and lipid metabolism were measured *ex vivo* in diaphragm or epididymal adipose tissue in absence (basal conditions) or presence of 250 µU/mL insulin (stimulated condition) in the incubation media. (L) Basal and adrenaline-stimulated lipolysis were measured in the epididymal adipose tissue in absence or presence of 250 µg/ml adrenaline. Number of animals: (A) 18 rats of each genotype; (B-L) 8 SHR-*Tti2*$^{+/-}$, 6 SHR. *p* values were derived from Student's *t*-test (A-H) or linear mixed effect model (I-L). Full details of statistical analysis are in Tables 2 and 3. Abbreviations: NEFA, non-esterified free fatty acids; TG, triglycerides.

bioRxiv preprint doi: https://doi.org/10.1101/2021.06.04.447058; this version posted June 4, 2021. The copyright holder for this preprint (which was not certified by peer review) is the author/funder, who has granted bioRxiv a license to display the preprint in perpetuity. It is made available under aCC-BY 4.0 International license.

285 **Table 2. Statistical comparison of neurogenesis and metabolic traits between SHR-**

286 ***Tti2*$^{+/-}$ rats and SHR wild type littermates.**

Phenotype	Unit	SHR	SHR-*Tti2*$^{+/-}$	*p* value
Neurogenesis	BrdU+ cells/DG	4143 ± 79	3266 ± 55	0.04 *
Body and organ weights				
Body weight	g	296.47 ± 2.62	308.41 ± 1.37	0.12
Relative weight of epid. fat	g/100 g bwt	0.69 ± 0.003	0.63 ± 0.005	0.0049 *
Relative weight of perirenal fat	g/100 g bwt	0.52 ± 0.01	0.58 ± 0.01	0.022 *
Relative weight of BAT	g/100 g bwt	0.09 ± 0.002	0.08 ± 0.002	0.71
Relative weight of liver	g/100 g bwt	3.48 ± 0.01	3.3 ± 0.01	0.0061 *
Relative weight of heart	g/100 g bwt	0.36 ± 0.003	0.35 ± 0.001	0.14
Relative weight of kidney	g/100 g bwt	0.69 ± 0.004	0.67 ± 0.002	0.028 *
Blood chemistry				
Non-fasting glucose	mmol/l	7.53 ± 0.07	6.94 ± 0.03	0.0057 *
Insulin	nmol/l	0.38 ± 0.02	0.22 ± 0.005	9.6e-5 *
Serum TG	mmol/l	0.36 ± 0.01	0.43 ± 0.01	0.048 *
Total cholesterol	mmol/l	1.13 ± 0.03	1.07 ± 0.01	0.39
HDL-C	mmol/l	1.04 ± 0.03	0.97 ± 0.01	0.27
NEFA	mmol/l	0.50 ± 0.01	0.61 ± 0.01	3.8E-4 *
Adiponectin	□g/ml	2.63 ± 0.36	2.33 ± 0.35	0.589
Leptin	ng/ml	3.20 ± 0.23	3.31 ± 0.12	0.692
Tissue composition				
TG in liver	µmol/g	6.49 ± 0.24	4.7 ± 0.12	0.016 *
Cholesterol in liver	µmol/g	10.93 ± 0.16	9.27 ± 0.07	0.0014 *
TG in heart	µmol/g	2.29 ± 0.08	0.71 ± 0.03	2.8E-6 *
TG in kidney	µmol/g	5.33 ± 0.21	5.57 ± 0.12	0.69
TG in muscle	µmol/g	1.35 ± 0.09	1.29 ± 0.06	0.80
Glucose and lipid metabolism				
Glucose oxidation in BAT	nmol glucose/g/2h	441.78 ± 19.17	386.76 ± 14.01	0.39
Basal lipogenesis in BAT	nmol glucose/g/2h	294.37 ± 11.14	262.82 ± 6.63	0.34
Basal lipogenesis in epid. fat $	nmol glucose/g/2h	481.05 ± 18.1	417 ± 8.62	0.80
Insulin-stimulated lipogenesis in epid. fat	nmol glucose/g/2h	717.14 ± 27.08	581.48 ± 23.12	0.23
Basal lipolysis in epid. fat	µmol NEFA/g	3.01 ± 0.05	3.51 ± 0.05	0.58
Adrenaline-stimulated lipolysis in epid. fat	µmol NEFA/g	6.09 ± 0.16	5.25 ± 0.13	0.15
Basal glycogenesis in diaphragm	nmol glucose/g/2h	892.26 ± 43.12	688.17 ± 30.06	0.37
Insulin-stimulated glycogenesis in diaphragm	nmol glucose/g/2h	1554.32 ± 35.04	701.84 ± 41.14	< 1E-4 *
Glucose oxidation in diaphragm	nmol glucose/g/2h	488.38 ± 20.66	343.98 ± 8.29	0.0042 *
Oxidative stress in the liver				
SOD activity	U/mg	0.16 ± 0.004	0.12 ± 0.003	0.026 *
GPx activity	µmol GSH/min/mg	293.14 ± 6.48	234.57 ± 5.26	0.021 *

bioRxiv preprint doi: https://doi.org/10.1101/2021.06.04.447058; this version posted June 4, 2021. The copyright holder for this preprint (which was not certified by peer review) is the author/funder, who has granted bioRxiv a license to display the preprint in perpetuity. It is made available under a CC-BY 4.0 International license.

GR activity	µmol NADPH/min/mg	132.14 ± 4.51	112.57 ± 2.52	0.18
CAT activity	µmol H_2O_2/min/mg	1260 ± 45.18	1522.14 ± 50.8	0.17
GSH/GSSG		39.64 ± 1.25	25.56 ± 0.97	0.0051*
GSH	µmol/mg	75.19 ± 1.18	72.94 ± 0.61	0.49
GSSG	µmol/mg	1.96 ± 0.07	3.15 ± 0.15	0.039 *
Conjugated dienes	nM/mg	35.29 ± 0.88	42.86 ± 0.71	0.027 *
TBARS	nM/mg	1.73 ± 0.06	1.36 ± 0.05	0.095

Table reports means ± standard errors of the mean. *p* values were derived from Student's *t*-test or post-hoc Tukey test following two-way mixed effect model with an interaction between genotype and stimulation as a fixed factor. Asterisks denote significance at $p < 0.05$. Abbreviations: BAT, brown adipose tissue; CAT, catalase; HDL-C, high-density lipoprotein bound cholesterol; epid., epididymal; GPx, glutathione peroxidase; GR, glutathione reductase; GSH, glutathione; GSSG, oxidised glutathione; NEFA, non-esterified fatty acids; SOD, superoxide dismutase; TBARS, thiobarbituric acid reactive substances; TG, triglycerides.

bioRxiv preprint doi: https://doi.org/10.1101/2021.06.04.447058; this version posted June 4, 2021. The copyright holder for this preprint (which was not certified by peer review) is the author/funder, who has granted bioRxiv a license to display the preprint in perpetuity. It is made available under a CC-BY 4.0 International license.

297 **Table 3. Statistical analysis of response to insulin and adrenaline stimulation in**

298 **tissues isolated from SHR-*Tti2*$^{+/-}$ rats and SHR wild type littermates.**

Phenotype	Term/Contrast	Statistic (d.f.)	*p*.value
Glycogenesis in diaphragm	Genotype	χ^2 (1) = 28.25	1.1E-7 *
	Insulin	χ^2 (1) = 9.72	0.0018 *
	Genotype:Insulin	χ^2 (1) = 11.03	9E-4 *
	SHR:250 – SHR:0	*t*(12) = 4.55	<1E-4 *
	SHR-*Tti2*$^{+/-}$:250 – SHR-*Tti2*$^{+/-}$:0	*t*(11) = 0.1	1
Glucose oxidation in diaphragm	Genotype	χ^2 (1) = 7.82	0.0052 *
	Insulin	χ^2 (1) = 1.34	0.25
	Genotype:Insulin	χ^2 (1) = 3.07	0.08
	SHR:250 – SHR:0	*t*(12) = 2.08	0.13
	SHR-*Tti2*$^{+/-}$:250 – SHR-*Tti2*$^{+/-}$:0	*t*(12) = -0.27	0.99
Lipogenesis in epididymal fat	Genotype	χ^2 (1) = 2.21	0.14
	Insulin	χ^2 (1) = 34.59	4.1E-9 *
	Genotype:Insulin	χ^2 (1) = 1.14	0.29
	SHR:250 – SHR:0	*t*(12) = 4.66	<1E-4 *
	SHR-*Tti2*$^{+/-}$:250 – SHR-*Tti2*$^{+/-}$:0	*t*(12) = 3.75	7.7E-4 *
Lipolysis in epididymal fat	Genotype	χ^2 (1) = 0.35	0.56
	Adrenaline	χ^2 (1) = 62.01	3.4E-15 *
	Genotype:Adrenaline	χ^2 (1) = 5.08	0.024 *
	SHR:250 – SHR:0	*t*(12) = 6.86	<1E-4 *
	SHR-*Tti2*$^{+/-}$:250 – SHR-*Tti2*$^{+/-}$:0	*t*(12) = 4.48	< 1E-4 *

299

300 Glucose and lipid metabolism were measured *ex vivo* in tissues isolated from SHR-*Tti2*$^{+/-}$ rats
301 and wild type SHR littermates under basal and induced conditions (without or with 250 µU/ml
302 insulin or 250 mg/ml adrenaline). The table shows results of two-way linear mixed effect
303 models with Insulin, Genotype and Insulin:Genotype interaction or Adrenaline, Genotype and
304 Adrenaline:Genotype as fixed effects and individual intercepts as a random effect. Statistical
305 significance was evaluated by likelihood ratio test. Adjusted *p* values for comparisons within
306 each genotype were obtained from *post-hoc* Tukey test for the interaction. Means and SEM
307 for each group and the comparison between genotypes are shown in Table 2. Asterisks
308 denote significance at $p < 0.05$; d.f., degrees of freedom.

309

bioRxiv preprint doi: https://doi.org/10.1101/2021.06.04.447058; this version posted June 4, 2021. The copyright holder for this preprint (which was not certified by peer review) is the author/funder, who has granted bioRxiv a license to display the preprint in perpetuity. It is made available under a CC-BY 4.0 International license.

Next, we investigated rates of glucose and lipid metabolism *ex vivo* in the skeletal muscle and adipose tissues from SHR-*Tti2*$^{+/-}$ and SHR control rats under basal conditions and upon stimulation. In the diaphragm, knock-out of *Tti2* abolished stimulatory effect of insulin on both glucose incorporation into glycogen, and glucose oxidation (Fig. 3I-J, see Tables 2 and 3 for detailed statistical analysis). However, the basal rates of glucose oxidation and glycogenesis in heterozygous rats were not significantly different from intact littermates. Similarly, basal glucose oxidation in BAT was not different between genotypes (Fig. S1M). In contrast to glucose utilisation in the skeletal muscle, incorporation of glucose into lipids in epididymal adipose tissue was significantly stimulated by insulin in both genotypes (Fig. 3K) and we did not detect differences between heterozygous and control rats in basal nor stimulated condition. *De novo* lipogenesis also did not differ between SHR-*Tti2*$^{+/-}$ and control rats in BAT (Fig. S1N). Furthermore, both SHR-*Tti2*$^{+/-}$ and SHR animals upregulated lipolysis in presence of adrenaline (Fig. 3L). However, a significant interaction between genotype and adrenaline stimulation suggested different response to stimulation depending on the *Tti2* expression level.

Metabolic deregulation and dyslipidaemia are often associated with elevated oxidative stress. We thus examined the hallmarks of the hepatic oxidative status. Indeed, significantly upregulated conjugated dienes in livers from heterozygous rats compared to control littermates (Fig. 4A) suggested increased oxidative stress. Increased oxidation was indicated also by decreased ratio of reduced to oxidised glutathione (GSH/GSSG; Fig. 4G), mostly due to increased concentrations of oxidised glutathione (GSSG; Fig. 4H). In contrast, the content of thiobarbituric acid reactive substances (TBARS) showed a decreasing trend (p = 0.095; Fig. 4B). The changes in lipid peroxidation were accompanied by decreased activity of the antioxidant enzymes, superoxide dismutase (SOD; Fig. 4C) and glutathione peroxidase (GPx; Fig. 4E). Glutathione reductase (GR; Fig. 4F) and catalase (CAT, Fig. 4D) were not significantly different between SHR-*Tti2*$^{+/-}$ and control littermates.

bioRxiv preprint doi: https://doi.org/10.1101/2021.06.04.447058; this version posted June 4, 2021. The copyright holder for this preprint (which was not certified by peer review) is the author/funder, who has granted bioRxiv a license to display the preprint in perpetuity. It is made available under a CC-BY 4.0 International license.

Fig. 4. Knock-down of Tti2 alters oxidative status in the liver.

Livers extracts prepared from three-months old heterozygous SHR-*Tti2*$^{+/-}$ rats (N = 7) and wild type SHR littermates (N = 7) were used to measure markers of oxidative stress as indicated in the figure. *p* values were derived from Student's *t*-test. Abbreviations: GSH, glutathione; GSSG, oxidised glutathione; TBARS, thiobarbituric acid reactive substances.

Together, these results indicate that lowering expression of functional full-length *Tti2* affected adult neurogenesis and metabolism, in particular glucose and insulin homeostasis, in agreement with *Tti2* being a causal gene underlying the joint neurogenesis and serum glucose QTL.

Gene expression profiles indicate glucose intolerance in SHR-*Tti2*$^{+/-}$ rats

The Tti2 protein, together with its binding partners, telomere maintenance 2 (Telo2) and Tti1, form a chaperone complex that assists folding and tertiary assembly of functional phosphatidylinositol 3-kinase-related kinases (PIKK): mammalian target of rapamycin (mTOR), ataxia telangiectasia mutated (ATM), ataxia telangiectasia and Rad3 related (ATR), suppressor of morphogenesis in genitalia (SMG1), transformation/transcription domain-associated protein (TRRAP) and DNA-dependent protein kinase catalytic subunit (DNA-PKcs) [50]. To get an insight into the molecular consequences of downregulation of *Tti2* expression, we performed transcriptional profiling of the hippocampus and three tissues essential for metabolic regulation in SHR-Tti2$^{+/-}$ rats and their wild-type littermates. We detected 326 differentially expressed transcripts in the liver, 52 in the soleus muscle, 41 in the perirenal fat, and 10 in the hippocampus. In addition, the analysis confirmed reduction of *Tti2* mRNA in the heterozygous rats (Table S3). We next carried out functional annotations using Ingenuity Pathway Analysis (IPA), which infers shifts in activity of canonical pathways and potential upstream regulators from the direction and magnitude of gene expression changes using curated knowledge databases. Furthermore, IPA can link differentially expressed genes to downstream outcomes.

bioRxiv preprint doi: https://doi.org/10.1101/2021.06.04.447058; this version posted June 4, 2021. The copyright holder for this preprint (which was not certified by peer review) is the author/funder, who has granted bioRxiv a license to display the preprint in perpetuity. It is made available under a CC-BY 4.0 International license.

We first checked whether observed gene expression changes could be connected to altered activity of any of the PIKK. Among canonical pathways, IPA indicated enrichment for genes associated with ATM signalling in the liver, muscle, and fat, and with mTOR signalling in the muscle (Fig. S2B-D). Additionally, IPA predicted SMG1 as one of potential upstream regulators in the liver and hippocampus (File S1). Nevertheless, the majority of changes in gene expression were not directly connected to PIKK activity.

In agreement with the metabolic phenotype of SHR-Tti2$^{+/-}$ rats, the transcriptional profile of the liver pointed to dysglycemia, specifically to decreased glucose tolerance and increased insulin resistance (Fig. 5A-B). IPA suggested four upstream regulators that could be linked to glucose intolerance: interleukin 6 (IL6), tuberous sclerosis complex 2 (Tsc2), peroxisome proliferator-activated receptor gamma coactivator 1-beta (Ppargc1b), and lysine (K)-specific histone demethylase 1A (Kdm1a) (Fig. S3). In addition, IPA indicated inhibition of insulin signalling as the most significant upstream regulator (File S2). The functional analysis also predicted a broad range of other metabolic changes, for example hepatic steatosis, decreased fatty acid metabolism and lipid synthesis (Fig. 5A, C; File S3). Even though only few differentially expressed genes were detected in the hippocampus of SHR-Tti2$^{+/-}$ rats, these genes indicated decreased cellular homoeostasis (Fig. 5A, D) and increased apoptosis. Very strong upregulation (24-times) of sphingosine1-phospate (S1P) receptor 3 (S1pr3) and downregulation of alkaline ceramidase 2 (Acer2) suggested de-regulation of S1P signalling pathway in the hippocampus (Fig. S2A).

Fig. 5. Functional analysis of gene expression changes indicates insulin resistance and loss of cellular homeostasis in SHR-*Tti2*$^{+/-}$ rats.

Differentially expressed genes between SHR-*Tti2*$^{+/-}$ rats and wild type SHR littermates in the liver, muscle, perirenal adipose tissue and hippocampus were analysed using Ingenuity Pathway Analysis (IPA). IPA predicts activation or inhibition of functions, pathological processes and molecular pathways from the direction and magnitude of expression changes using curated databases. (A) Graph depicts activation (positive Z-score) or inhibition

bioRxiv preprint doi: https://doi.org/10.1101/2021.06.04.447058; this version posted June 4, 2021. The copyright holder for this preprint (which was not certified by peer review) is the author/funder, who has granted bioRxiv a license to display the preprint in perpetuity. It is made available under a CC-BY 4.0 International license.

(negative Z-score) of top functions and diseases in each of the analysed tissues. Full list of significantly affected functions can be found in File S3. (B-D) Edges in each network illustrate predicted relationships between upregulated (magenta) and downregulated (green) genes and downstream functions (centre nodes; orange, activating effect; blue, inhibitory effect). (E) Colour key. Asterisks in network graphs denote multi-protein complexes.

Human genomic variation links *TTI2* expression with genome-wide phenotype associations

Our results indicated that changes in expression levels of *Tti2* can affect both neural and metabolic homeostases. The majority of disease-associated variants in humans are likely to be involved in regulation of transcription [51,52]. Therefore, to link our findings to genomic variation in the human population, we searched the human eQTL catalogue (https://www.ebi.ac.uk/eqtl/) for variants associated with changes in the *TTI2* mRNA expression. We extracted 821 variants underlying 2177 eQTL (p < 1e-4) in 28 different tissues and cell types (File S4). Out of these, 214 variants were associated with the *TTI2* eQTL in at least 3 distinct tissue types (Fig. S4). The multi-tissue eQTL are more likely to represent true associations as well as being consequential for a wide range of phenotypes [16,17]. We next used all *TTI2* eQTL variants to query the GWAS databases (https://www.ebi.ac.uk/gwas/) for known phenotypic associations. We found 7 variants with reported associations to protein and stem cell factor blood concentrations, blood pressure and frontotemporal dementia (Table 4).

bioRxiv preprint doi: https://doi.org/10.1101/2021.06.04.447058; this version posted June 4, 2021. The copyright holder for this preprint (which was not certified by peer review) is the author/funder, who has granted bioRxiv a license to display the preprint in perpetuity. It is made available under aCC-BY 4.0 International license.

Table 4. Human genomic variants with overlapping associations to *TTI2* expression and phenotypes.

Variant ID	eQTL beta direction	eQTL data sets	Associated trait	Trait ID	GWAS *p* value	GWAS beta direction	Risk Frequency*
rs10094645	increase	Artery_Aorta, Muscle_Skeletal, Testis, Thyroid, Whole_Blood	blood protein measurement	EFO_0007937	4E-23	decrease	0.594
rs2732317	increase	Artery_Aorta, Testis, Thyroid, Whole_Blood	blood protein measurement	EFO_0007937	3E-77	decrease	0.612
rs2732260	increase	Monocyte	frontotemporal dementia, memory impairment	Orphanet_282 EFO_0001072	1E-6	NA	0.03
rs2732259	increase	Esophagus_Muscularis, Muscle_Skeletal, Testis, Whole_Blood	hypoxanthine measurement	EFO_0010500	7E-6	increase	0.619*
rs6996562	increase	Artery_Aorta, Testis, Whole_Blood	pulse pressure measurement	EFO_0005763	2E-10	increase	0.473
rs7845722	increase	Artery_Aorta, Muscle_Skeletal, Testis, Whole_Blood	pulse pressure measurement	EFO_0005763	1E-9	increase	0.4
rs1568119	decrease	Monocyte	stem cell factor measurement	EFO_0008291	1E-7	increase	0.08*

821 variants linked to *TTI2* eQTLs (p < 1E-4) were used to search human genome-wide association studies (GWAS) catalogue. *Data sets* column lists tissues and cell types in which significant eQTLs were detected for a given variant. For GWAS studies for which risk frequencies were not reported, we included variant frequencies from phase 3 1000 Genomes Project combined population (denoted with asterisks).

bioRxiv preprint doi: https://doi.org/10.1101/2021.06.04.447058; this version posted June 4, 2021. The copyright holder for this preprint (which was not certified by peer review) is the author/funder, who has granted bioRxiv a license to display the preprint in perpetuity. It is made available under aCC-BY 4.0 International license.

423

bioRxiv preprint doi: https://doi.org/10.1101/2021.06.04.447058; this version posted June 4, 2021. The copyright holder for this preprint (which was not certified by peer review) is the author/funder, who has granted bioRxiv a license to display the preprint in perpetuity. It is made available under a CC-BY 4.0 International license.

Discussion

In this study we used unbiased systems genetics methods to i) discover a number of metabolic and endocrine genetic correlates of the two critical parameters of adult hippocampal neurogenesis—precursor cell proliferation and net neurogenesis; and ii) identify *Tti2* as a molecular link between brain cellular plasticity and peripheral metabolism.

The HXB/BXH family is well-suited to discover genetic physiological correlates of cognitive endophenotypes

The HXB/BXH family of 30 members has only modest statistical power to detect QTL, as the majority of loci have only small effects on phenotypes and variants behind a substantial part of heritability fall below stringent significance levels. Nonetheless, the chief advantage of recombinant inbred strains is their suitability to measure the tendency of traits to co-segregate [44]. Because each inbred line can supply an indefinite number of isogenic individuals, multiple phenotypes can be measured in the same genotype, the collected data are cumulative and comparable across time and laboratories. Use of separate cohorts of animals to assess different phenotypes precludes intra-individual correlations and ensures that any associations between traits are due to shared genetic variation. Genetic correlations, therefore, may suggest the presence of allelic variants with pleiotropic effects on correlating phenotypes. Here we showed that, under basic laboratory conditions, precursor cell proliferation and the final outcome of adult neurogenesis—numbers of surviving neurons—are under the control of largely distinct sets of genes. Accordingly, each of these traits correlated to non-overlapping collections of metabolic and endocrine parameters. Because adult neurogenesis—although a complex process in itself—represents one specific aspect of brain plasticity, these correlations advance our understanding of interactions between global metabolic features and cognition. Here we proceeded to dissect in-depth the correlation between serum glucose and net neurogenesis, which could both be mapped to a common overlapping QTL. The majority of discovered correlations, however, could not be explained by such a strong genetic association, in agreement with the polygenic nature of

bioRxiv preprint doi: https://doi.org/10.1101/2021.06.04.447058; this version posted June 4, 2021. The copyright holder for this preprint (which was not certified by peer review) is the author/funder, who has granted bioRxiv a license to display the preprint in perpetuity. It is made available under a CC-BY 4.0 International license.

quantitative traits. Other methods, such as gene co-expression analyses, have the potential to integrate available data and elucidate mechanisms underlying remaining relationships [32].

Tti2 as a pleiotropic gene regulating net neurogenesis and metabolic homeostasis

Using transcriptional profiles from peripheral tissues and the hippocampus as intermediate phenotypes between complex physiological outcomes and genomic variation we were able to narrow down the 'serum glucose-neurogenesis' QTL interval to the *Tti2* candidate gene. Tti2, together with its binding partners, Tti1 and telomere maintenance 2 (Telo2) protein, form the Triple T (TTT) complex [53], which associates with a number of molecular chaperones, including Hsp90, Hsp70, Hsp40, and the R2TP/prefoldin-like complex [54,55]. TTT binds to nascent peptides of PI3K-related protein kinases (PIKK) and thereby acts as a specialised chaperone and a critical regulator of PIKK abundance in mammalian and yeast cells [53,55–58]. In mammals, the PIKK family consists of ATM, ATR, mTOR, TRAPP, SMG1, and DNA-PKcs. These proteins play strategic roles in multiple cellular functions, such as genome stability, DNA repair, regulation of gene and protein expression, nonsense-mediated RNA decay, cell growth and cell cycle progression, and regulation of responses to nutrient availability [59–62]. All PIKK are also an important part of stress responses [63].

In our present study, we generated a heterozygous SHR-*Tti2*$^{+/-}$ line carrying a frame-shift mutation in the N-terminal domain of *Tti2.* Mutational screens in yeast produced viable cells only when truncations were located at the very end of the C-terminus of *Tti2* [64], hence we predicted that this modification results in a non-functional protein. Our aim was to mirror the eQTL effect and reduce the amount of available Tti2 rather than remove it completely. The SHR background had been chosen because the SHR allele is associated with higher *Tti2* expression. The mutation halved the *Tti2* mRNA content in heterozygous rats compared to the wild-type littermates, as established by RNA sequencing. Although antibodies recognising rodent Tti2 were not available, experiments in yeast have suggested that the Tti2 protein abundance is directly correlated to mRNA expression [53]. SHR-*Tti2*$^{+/-}$ rats had

bioRxiv preprint doi: https://doi.org/10.1101/2021.06.04.447058; this version posted June 4, 2021. The copyright holder for this preprint (which was not certified by peer review) is the author/funder, who has granted bioRxiv a license to display the preprint in perpetuity. It is made available under a CC-BY 4.0 International license.

similar body weights, gross morphology and general cage behaviour as the wild-type littermates. However, reducing *Tti2* expression to 50% led to a reduction of the number of new neurons in the DG, a concomitant lowering of serum glucose and insulin concentrations, and to hallmarks of insulin resistance in skeletal muscles. Metabolic alterations in SHR-*Tti2*$^{+/-}$ rats went beyond glucose homeostasis: we also observed changes in lipid metabolism and elevated oxidative stress in the liver. Together, these findings support *Tti2* as a causal gene within the joint 'serum glucose-neurogenesis' QTL.

Expression of *Tti2* correlated negatively to adult neurogenesis and serum glucose concentrations in the HXB/BXH family, yet in the SHR rats with only one functional copy of the *Tti2* gene we saw a further decrease of each trait value. This disparity would imply that the SHR allele is associated with decrease of the Tti2 protein function despite higher *Tti2* mRNA abundance. The SHR allele carries six amino-acid substitutions, including Glu247Asp within the highly conserved Tti2 family super-helical central domain (conservation score 1.0; see Supplementary Table 1) and Lys198Glu at a moderately conserved residue (score 0.57) in the N-terminal portion of the protein. Although all substitutions were scored as benign by prediction algorithms SIFT and PolyPhen, it cannot be excluded that they have an impact on protein stability or interactions with any of the binding partners. Higher mRNA expression could evolve independently or as a compensation of reduced function. For example, in the duplicated maize genome, the number of copies of genes encoding TTT complex members and PIKK have all reverted to one, suggesting evolutionary pressure to maintain gene dosage balance [65].

Transcriptome profiling of SHR-*Tti2*$^{+/-}$ rats revealed extensive gene expression changes in the liver, and to a lesser degree in the skeletal muscle, perirenal fat and hippocampus compared to SHR wild type littermates. Liver, together with skeletal muscle and adipose tissue are decisive organs in maintenance of glucose homeostasis and hence development of insulin resistance [66]. Functional analysis of differentially expressed genes in the liver identified networks of genes and potential regulators whose activation and inhibition could explain insulin resistance and dysglycemia in the heterozygous animals. We also recorded

bioRxiv preprint doi: https://doi.org/10.1101/2021.06.04.447058; this version posted June 4, 2021. The copyright holder for this preprint (which was not certified by peer review) is the author/funder, who has granted bioRxiv a license to display the preprint in perpetuity. It is made available under a CC-BY 4.0 International license.

significant upregulation of *Insr* in the muscle, which IPA interpreted as consistent with hypoglycaemia and insulin resistant diabetes (File S3).

We also used IPA to predict which upstream regulators could be activated or inhibited in a manner consistent with observed gene expression changes. The vast majority of differentially expressed genes were not linked to PIKK activity. Thus far only PIKK peptides were identified as clients of the TTT complex despite attempts to capture other target proteins [64]. Therefore it is unlikely that another, yet unknown, pathway contributes to the observed phenotypes. Depletion of Tti2 destabilises all PIKK proteins and impairs nuclear localisation of ATM, ATR and TRRAP, but does not affect their mRNA abundance [53,64]. Notwithstanding the lack of direct evidence, reduction of *Tti2* expression in SHR-*Tti2*$^{+/-}$ rats may destabilise the TTT complex and consequently impair signalling of PIKK. It has been reported that reduced PIKK signalling due to tissue-specific targeting of selected genes in the mouse led to impaired adipogenesis (reduced fat deposits), insulin resistance with lower insulin-stimulated glucose transport, reduced antilipolytic effects of insulin (increased NEFA levels), and ectopic fat accumulation [67–71]. These results are similar to metabolic disturbances observed in SHR-*Tti2*$^{+/-}$ rats suggesting involvement of the same molecular pathways. Our data also do not allow differentiating whether all or only some of the PIKK are compromised in the SHR-*Tti2*$^{+/-}$ rats. Destabilisation of the TTT complex has strongest effects on ATM and ATR protein levels and to a lesser extent other PIKK [53,58,64,72]. Interestingly, in SHR-*Tti2*$^{+/-}$ rats IPA detected enrichment of differentially expressed genes related to ATM signalling in the liver, muscle and fat and mTOR signalling in the muscle. While these results do not imply that other PIKK were not affected, ATM might be the most sensitive to Tti2 downregulation also in rats used in our study.

Pleiotropy occurs when a single genomic variation, or more broadly a change in a function of a single gene, has multiple consequences at the phenotypic level [9]. Because metabolic diseases can, to some extent, be modified by lifestyle interventions in order to prevent or dampen cognitive decline, but genes cannot, it is clinically crucial to understand which correlations between metabolic and cognitive phenotypes arise from genetic predisposition

bioRxiv preprint doi: https://doi.org/10.1101/2021.06.04.447058; this version posted June 4, 2021. The copyright holder for this preprint (which was not certified by peer review) is the author/funder, who has granted bioRxiv a license to display the preprint in perpetuity. It is made available under a CC-BY 4.0 International license.

534 due to pleiotropic genes. Because we used targeted mutagenesis at the *Tti2* locus rather
535 than tissue specific approaches to confirm association with target phenotypes, we cannot
536 exclude that Tti2 affects neurogenesis through circulating metabolites or hormones.
537 Correlations between traits in the absence of genetic variation indicate indirect effects [10].
538 Hippocampal plasticity and neurogenesis are intricately related to nutrient availability and
539 insulin and insulin-like growth factor 1 (IGF1) signalling [73–76]. Glucose is the primary
540 energy source for the nervous system. Hyperglycemia and insulin resistance are detrimental
541 to the brain and negatively influence adult hippocampal neurogenesis [77–80]. In addition,
542 caloric restriction, which lowers plasma insulin and glucose levels, resulted in increased
543 survival of new neurons and higher net neurogenesis [81]. These associations hint that, as
544 such, the lower serum glucose measured in SHR-*Tti2*$^{+/-}$ rats may not necessarily lead to
545 lower neuronal survival. In the HXB/BXH family, neurogenesis correlated positively to serum
546 insulin (Pearson's $r = 0.35$, $p = 0.09$). However, we did not detect any consistent associations
547 with measures of insulin resistance, suggesting that peripheral insulin resistance is also
548 unlikely a sole cause of neurogenesis impairment in SHR-*Tti2*$^{+/-}$ rats. Furthermore,
549 transcriptional profiling of the hippocampus from heterozygous animals did not indicate brain
550 insulin resistance. Metabolic tissues in heterozygous rats also manifested deregulated lipid
551 metabolism. Higher levels of circulating triglycerides and free fatty acids could further
552 contribute to disrupted glucose metabolism and neurogenesis. For example, high fat diets,
553 which increase circulating plasma lipids and lipid peroxidation, have been documented as
554 detrimental to neurogenesis and cognition [82,83].

555 The support in favour of direct effects of Tti2 reduction on neurogenesis comes from the
556 severe neural deficits in individuals carrying loss-of-function mutations in *TTI2* in the absence
557 of serious metabolic insufficiencies. In humans, homozygous and compound heterozygous
558 loss-of-function mutations in *TTI2* cause microcephaly, severe intellectual disability,
559 dysmorphic facial features, short stature, speech and movement disorders, and skeletal
560 deformations [72,84–86]. Similar abnormalities were observed in children carrying *TELO2*
561 mutations [87,88]. Particularly, failures of DNA repair pathways downstream of the TTT

bioRxiv preprint doi: https://doi.org/10.1101/2021.06.04.447058; this version posted June 4, 2021. The copyright holder for this preprint (which was not certified by peer review) is the author/funder, who has granted bioRxiv a license to display the preprint in perpetuity. It is made available under a CC-BY 4.0 International license.

562 complex have detrimental effects on development and maintenance of the central nervous
563 system. Recessive mutations in ATM cause ataxia telangiectasia, a disease characterised by
564 progressive neuronal degeneration [89,90]; while loss of ATR leads to Seckel syndrome
565 characterised by postnatal dwarfism, microcephaly, intrauterine growth defects, and mental
566 retardation [91]. ATM, ATR and DNA-PKcs are essential to preserving the genome integrity
567 during replication [92] and thus their function is particularly important in dividing precursor
568 cells in the course of neurogenesis [93], also in the adult hippocampus [94]. Knock-out of
569 ATM or ATR in mice has detrimental effects on brain development, with pronounced loss of
570 hippocampal neurons [95]. ATM-deficient mice have abnormally increased rates of
571 proliferation with concomitantly lowered survival of new neurons [94]. In human neural stem
572 cells, ATM suppresses excessive retrotransposition [96], the process which contributes to
573 neural diversity and plasticity during hippocampus development, and then in the adult stem
574 cells [97].

575 mTOR also plays multiple roles in the development and function of the brain [98],
576 including maintenance of neural progenitor cell pools. During embryonic development,
577 conditional knockout of mTOR in neural stem cells dramatically reduced their proliferation
578 thereby reducing production of postmitotic neurons and brain size [99]. Similarly, inhibition of
579 mTORC1 signalling in the neural stem cells in the neonatal subventricular zone (SVZ) of the
580 lateral ventricle, which also harbours a population of neural stem cells that persist throughout
581 life, reduced generation of transient amplifying precursor cells and thus decreased the
582 abundance of their differentiated progeny [100]. In addition, transient systemic inhibition of
583 the mTOR pathway by rapamycin in early postnatal life resulted in abnormal proliferation,
584 reduced progenitor cell numbers, and eventually decreased the volume of the adult dentate
585 gyrus [101].

586 ATM and mTOR are both downstream targets of insulin and IGF1 signalling [89]. Insulin
587 and IGF1 provide trophic signals that can both stimulate and inhibit proliferation and survival
588 of adult precursor cells *in vivo* [74,102–107]. Insulin is also expressed directly in neuronal
589 progenitors [108]. The massive upregulation of S1pr3 and downregulation of Acer2 in the

bioRxiv preprint doi: https://doi.org/10.1101/2021.06.04.447058; this version posted June 4, 2021. The copyright holder for this preprint (which was not certified by peer review) is the author/funder, who has granted bioRxiv a license to display the preprint in perpetuity. It is made available under a CC-BY 4.0 International license.

hippocampus of SHR-*Tti2*$^{+/-}$ rats suggested changes in the sphingosine-1-phosphate (S1P) signalling pathway, which is implicated in the control of cell death and survival, as well as synaptic plasticity via interactions with multiple cellular signalling cascades [109–112]. Interestingly, S1pr3 potentiates IGF1 signalling [113], and cross-links with the mTOR-AKT nutrient sensing pathway [114]. Although our analysis of differentially expressed genes did not suggest changes in PIKK activity in the hippocampus of heterozygous animals, the precursor cells and immature neurons are only a minor fraction of the entire hippocampus and therefore we might not have captured genes affected specifically in these cells. For example, Ka and colleagues [99] found that in the developing cerebral cortex mTOR signalling was detected mostly in the radial neural stem cells, the principal precursor cells of the developing central nervous system, with very low activity in the postmitotic neuronal layers. In the early postnatal and adult SVZ, mTOR activity was also concentrated in actively proliferating transient amplifying progenitor cells [100,115]. All told, the interwoven relationships between peripheral metabolism, insulin and PIKK signalling pathways point to complex responses to intracellular deficits in PIKK and extracellular signals in the brain of SHR-*Tti2*$^{+/-}$ rats, and lend support for truly pleiotropic roles of *Tti2* in the regulation of glucose homeostasis and structural brain plasticity. Future development of tissue- and cell-specific conditional knockouts shall help to decipher the consequences of *Tti2* depletion for these functions independently of each other.

Limitations

In our study we used only male rats. This decision was dictated by compatibility with existing data, as the vast majority of published HXB/BXH phenotypes were measured in young male rats to avoid inter-individual variation due to oestrous cycle. Further experiments will show whether any of the identified associations interacts with sex.

bioRxiv preprint doi: https://doi.org/10.1101/2021.06.04.447058; this version posted June 4, 2021. The copyright holder for this preprint (which was not certified by peer review) is the author/funder, who has granted bioRxiv a license to display the preprint in perpetuity. It is made available under a CC-BY 4.0 International license.

Conclusion

Understanding of the molecular events by which a genomic variation leads to physiological consequences for the organism across many functions provides a foundation for effective precision medicine. Our study exemplifies the power of rodent genetic reference populations not only to identify associations between phenotypes that are difficult or even impossible to assess in humans, but also to give insights into the cell biology behind these associations. Our experiments showed that manipulating the abundance of a single component of the protein folding machinery had relatively subtle yet significant effects on a broad range of phenotypes. Mining human data sets revealed more than 800 genomic variants that are linked to *TTI2* expression, seven of which refer to associations with protein and blood stem cell factor concentrations, blood pressure, and frontotemporal dementia. Given the dose-dependent effects of *Tti2* on adult hippocampal neurogenesis and glucose homeostasis, we speculate that human variants that affect *TTI2* expression or function may also have quantitative effects on these phenotypes.

Acknowledgments

The authors would like to thank Karel Vales, Michaela Radostna, Hana Brozka, Jan-Hendrik Claasen, Perla Leal-Galicia, Tara L. Walker, and Sara Zocher for assistance with perfusions; Anna Rumiantseva for help with histological staining; Vladimir Landa for microinjecting fertilised ova with the ZFN construct; Olena Oliyarnyk for oxidative stress analysis; Edwin Cuppen, Marieke Simonis, Kathrin Saar, and Oliver Hummel for SHR genomic variants and genotype information.

Funding

This work was supported by DFG (KE 615/9-1) (ANG, GK), EnergI (ANG, GK) and basic TUD and DZNE institutional funding (ANG, RWO, KSF, GK). MP and HM were supported by the Ministry of Health of the Czech Republic under the conceptual development of research

bioRxiv preprint doi: https://doi.org/10.1101/2021.06.04.447058; this version posted June 4, 2021. The copyright holder for this preprint (which was not certified by peer review) is the author/funder, who has granted bioRxiv a license to display the preprint in perpetuity. It is made available under a CC-BY 4.0 International license.

639 organizations program (Institute for Clinical and Experimental Medicine – IKEM, IN 00023001
640 (HM) and by the Academic Premium (Praemium academiae) (AP1502) (MP); AS was
641 supported by Czech Health Research Council (AZV) grant 17-30833A and Czech Science
642 Foundation (GACR) projects 19-03016S and 20-00939S.
643

bioRxiv preprint doi: https://doi.org/10.1101/2021.06.04.447058; this version posted June 4, 2021. The copyright holder for this preprint (which was not certified by peer review) is the author/funder, who has granted bioRxiv a license to display the preprint in perpetuity. It is made available under aCC-BY 4.0 International license.

Materials and Methods

Animals

Brown Norway BN-*Lx*/Cub, spontaneously hypertensive SHR/OlaIpcv (referred to as BN and SHR, respectively) and 30 HXB/BXH recombinant inbred strains, as well as SHR-*Tti2*$^{+/-}$ knockout heterozygous rats used in the current study were housed in an air-conditioned animal facility at the Institute of Physiology, Czech Academy of Sciences. HXB/BXH strains are inbred for more than 80 generations. Animals were maintained on a 12 h light/dark cycle in the standard laboratory cages provided with standard laboratory chow and water *ad libitum*. To assess survival of new-born cells in the dentate gyrus, 10-week-old animals were given 3 daily intraperitoneal injections of 50 mg/kg bromodeoxyruidine (BrdU; Sigma) and perfused 28 days later. We studied 5–9 male rats from each strain derived from at least 3 independent litters (total 243 rats). To isolate tissues for RNA and protein isolation, rats were anaesthetised with ketamine and decapitated. Tissues were placed in RNA later (microarray) or snap frozen in liquid nitrogen. For the microarray analysis, one male and one female 10-week-old rat from each parental and HXB/BXH strains were used (total 64 rats). Biochemical, metabolic and hemodynamic phenotypes were assessed in 3-month-old non-fasted male SHR-Tti2$^{+/-}$ rats and their wild-type littermates (N = 8 per strain). All experiments were performed in agreement with the Animal Protection Law of the Czech Republic and were approved by the Ethics Committee of the Institute of Physiology, Czech Academy of Sciences, Prague (Permit number: 66/2014).

Generation of Tti2 knockout SHR rats.

Tti2 knockout rats were generated by microinjecting fertilized ova of SHR rats with the ZFN (Zinc Finger Nuclease) construct from Sigma-Aldrich. The construct was designed to target the first exon using the following sequence of ZFN binding (capital letters) and cutting site (small letters): TCTGACCCGGATCCAAGCaccaagGGTGGGTGGCAGGGC. DNA samples isolated from 452 rats born after microinjection with ZFN construct were amplified

bioRxiv preprint doi: https://doi.org/10.1101/2021.06.04.447058; this version posted June 4, 2021. The copyright holder for this preprint (which was not certified by peer review) is the author/funder, who has granted bioRxiv a license to display the preprint in perpetuity. It is made available under a CC-BY 4.0 International license.

using primers flanking the target sequence: ZFN F: 5'-TACACTGTGATTGGCTGGGA-3' and ZFN R: 5'-GGCGCAGTGGAGTGATC-3'. Altogether 4 positive animals were detected. An SHR-*Tti2*^{tm1}/Ipcv line no.14 (referred to as SHR-*Tti2*$^{+/-}$) with an 8 bp deletion (NM_001013883.1(Tti2):c.243_250delCGAGATCC; on the protein level: NP_001013905.1:p.Glu82Glyfs) has been selected for further analyses. The heterozygous founder was crossed with SHR and F1 rats were intercrossed. SHR-*Tti2*$^{+/-}$ heterozygotes were selected for breeding and phenotyping while their wild type littermates were used as controls.

Histology

Histology was carried out using standard procedures [45]. Rats were deeply anaesthetised with a mixture of ketamine/xylazine and intracardially perfused with 0.9% NaCl, followed by ice-cold 4 % paraformaldehyde (PFA) in 0.1 M phosphate buffer (PB), pH 7.4. The brains were removed, post-fixed overnight in 4 % PFA and equilibrated in 30 % w/v sucrose in 0.1 M phosphate buffer. 40 µm frozen coronal sections were cut on a sliding microtome (Leica) and stored in a cryo-protective solution (25 % ethylene glycol, 25 % glycerol in 0.1 M PB) at –20 □C.

For immunohistochemistry, every sixth section was washed in Tris-buffered saline (TBS) and pretreated in 3 % H_2O_2 and 10 % methanol in TBS for 15 min. After several washes in TBS and NaCl, DNA was denatured with 2.5 M HCl for 30 min at 37 □C. Multiple washes in phosphate-buffered saline (PBS) were performed between each subsequent step. The sections were incubated in a blocking solution containing 10 % donkey serum and 0.3 % Triton-X100 in PBS for 1 h and then with primary antibodies (rat anti-BrdU, 1:500, OBT0030, AbD Serotec; or rabbit anti-Ki67, 1:500, NCL-Ki67p, Novocastra) diluted in the blocking solution for 48 – 72 h at 4 □C. Sections were incubated for 2.5 h with biotinylated secondary antibodies (1:500, Jackson ImmunoResearch) diluted in the blocking solution containing 3 % donkey serum. Immunocomplexes were detected using the Vectastain Elite ABC kit (Vector Laboratories) and 0.02 % diaminobenzidine (D5905, Sigma) enhanced with $NiCl_2$. After

bioRxiv preprint doi: https://doi.org/10.1101/2021.06.04.447058; this version posted June 4, 2021. The copyright holder for this preprint (which was not certified by peer review) is the author/funder, who has granted bioRxiv a license to display the preprint in perpetuity. It is made available under a CC-BY 4.0 International license.

mounting in 0.1 M PB onto gelatine-coated glass slides, the sections were air dried, cleared in the alcohol gradient series, and coverslipped with Entellan New (Merck).

Cells were quantified using a simplified optical fractionator method as discussed before [Kempermann 2003 PMID: 12466205]. BrdU positive cells were quantified along the rostro-caudal axis in the granule cell layer (GCL) and subgranular zone (SGZ) defined as a two-cell wide band below the GCL. Ki67 cells were quantified in the three-cell wide zone below the GCL and in the inner third of the GCL. Clusters of cells were defined as at least three cells not further apart than two-cell diameter. The cells in the uppermost focal plane were ignored to avoid oversampling errors. The counts from left and right sides of the DG in each sample were averaged and multiplied by 6 (section sampling interval) to obtain total numbers of newborn (BrdU) or proliferating (Ki67) cells in per dentate gyrus.

To assess the identity of BrdU-positive cells and estimate the range of neuronal and astrocyte survival across the HXB/BXH family, sections from three randomly selected individuals from each parental strain and one from each HXB/BXH member were processed for fluorescent staining with BrdU, NeuN and S100□. Every twelfth section was washed twice in NaCl, pretreated in 2 M HCl for 30 min at 37 □C and washed in PBS. After blocking, sections were incubated for 48 h at 4 □C with primary antibodies (rat anti-BrdU, 1:500, OBT Serotec; mouse anti-NeuN, 1:200, MAB377, Millipore; rabbit anti-S100□, 1:2000, Ab41548, Abcam) diluted in the blocking solution. After washing in PBS, sections were incubated for 4 h with secondary antibodies (anti-rat Cy3, anti-mouse DyLight 488, anti-rabbit Cy5, 1:500, Jackson Immunoresearch) diluted in the blocking solution, washed in PBS and mounted onto glass slides using fluorescence mounting medium Aqua-Poly/Mount (Polysciences). 100 randomly selected BrdU-positive cells from each animal along the rostro-caudal axis of the DG were imaged at 400□ magnification with spectral confocal microscope (TCS SP2, Leica) and examined for NeuN and S100□ immunoreactivity.

bioRxiv preprint doi: https://doi.org/10.1101/2021.06.04.447058; this version posted June 4, 2021. The copyright holder for this preprint (which was not certified by peer review) is the author/funder, who has granted bioRxiv a license to display the preprint in perpetuity. It is made available under a CC-BY 4.0 International license.

722 **Microarray analysis**

723 Hippocampi were dissected from brains stored in RNA later and RNA was isolated using
724 RNA STAT-60 kit (Tel-Test Inc). RNA was purified using standard sodium acetate-ethanol
725 precipitation method. RNA purity and concentration was evaluated using 260/280 nm
726 absorbance ratio and the quality was checked using Agilent Bioanalyzer 2100 prior to
727 hybridisation. Samples were hybridised onto GeneChip Rat Exon 1.0 ST microarrays
728 (Affymetrix) using manufacturers protocols.

729 Along with the hippocampus gene expression data, we analysed published data sets from
730 parental and 29 recombinant inbred strains from adrenal gland, liver, skeletal muscle,
731 perirenal fat, kidney, aorta and ventricle [37,38,40]. These data sets consisted of microarray
732 analysis on Affymetrix Rat230_2 (muscle, liver, aorta and ventricle) and RAE230A (adrenal
733 gland, fat and kidney) chips. Unprocessed microarray expression data were retrieved from
734 ArrayExpress, (www.ebi.ac.uk/arrayexpress; adrenal gland, E-TABM-457; liver, E-MTAB-
735 323; muscle, E-TABM-458; fat and kidney, E-AFMX-7; aorta, E-MTAB-322; left ventricle, E-
736 MIMR-222).

737 Probes from each data set were assembled into probesets mapped to Ensemble gene
738 identifiers from Rnor_5.0 rat genome release using Version 10 custom cell definition files
739 from the Brain Array (University of Michingan) website [116]. Probes that mapped to regions
740 containing insertions, deletions or single nucleotide polymorphisms in the SHR/Ola or BN-
741 *Lx*/Cub strains compared to the reference genome [43] were removed prior the analysis to
742 avoid spurious linkage due to differential hybridisation. Probesets which after filtering
743 contained less than 3 probes were removed. Gene expression summaries were derived
744 using robust multichip average (RMA) algorithm [117] in the R Affy package [118].

745 **Heritability**

746 In repeated sampling of isogenic individuals, the variance observed within the genotype
747 can be attributed to environmental influences, whereas differences between strains are
748 primarily due to differences in genotypes. Thus, we defined narrow sense heritability as the

bioRxiv preprint doi: https://doi.org/10.1101/2021.06.04.447058; this version posted June 4, 2021. The copyright holder for this preprint (which was not certified by peer review) is the author/funder, who has granted bioRxiv a license to display the preprint in perpetuity. It is made available under a CC-BY 4.0 International license.

intraclass correlation coefficient obtained from a mixed linear model employing restricted maximum likelihood approach using function *lmer* from lme4 R package [119,120].

QTL mapping

Phenotype QTL were calculated using strain means for surviving ($BrdU^+$) and proliferating ($Ki67^+$) cells in the DG as well as for phenotypes correlating to neurogenesis traits. Expression QTL (eQTL) were calculated for all genes in each data set. Marker regression against SNP-based genotype markers mapped to Rnor_5.0 genome assembly with 2049 unique strain distribution patterns in 29 HXB/BXH strains [121] was performed using the QTLReaper program [122], which reports likelihood ratio statistic (LRS) score at each marker. LRS was converted to logarithm of odds ratio (LOD) by dividing by 4.61, where $LOD \approx -log_{10}(p)$. Empirical genome-wide significance of linkage was determined by a permutation test as previously described [37]. Genome wide significance was defined as the 95th percentile of the maximum LOD score and less stringent suggestive threshold as the 37th percentile, which on average yields one false positive per genome scan [123,124]. The 95 % confidence intervals for QTL were calculated in R/qtl using Bayesian method [125]. Traits with overlapping QTL were summarised as their first principal component, an eigenphenotype (adult neurogenesis and serum glucose) or eigengene (*Tti2* expression), using WGCNA R package [126]. eQTL were defined as local when position of a QTL mapped within 10 Mb from the physical location of the gene [37]. Conditional genome scans were carried out in R/qtl as described previously [47–49] to establish relationships between genomic loci, gene expression and phenotypes using function *scanone* with parameter *addcovar*. The gene was considered causal when the LOD score of the phenotype QTL fell below suggestive level after conditioning on its expression. Analysis of mutations of candidate genes was performed using tools in Rat Genome Database [127]. All genomic positions were mapped to Rnor_5.0 genome assembly.

bioRxiv preprint doi: https://doi.org/10.1101/2021.06.04.447058; this version posted June 4, 2021. The copyright holder for this preprint (which was not certified by peer review) is the author/funder, who has granted bioRxiv a license to display the preprint in perpetuity. It is made available under aCC-BY 4.0 International license.

774 **RNA isolation and quantitative PCR**

775 RNA was isolated using RNeasy Mini Kit (Qiagen) following manufacturer's instructions.
776 Genomic DNA was removed by on-column DNase digestion. Frozen tissues were
777 homogenised in QIAzol with TissueRuptor (Qiagen). cDNA was synthesised with SuperScript
778 II reverse transcriptase (Invitrogen) using oligo(dT) primers and 1 µg of total RNA.
779 Quantitative PCR was performed using SYBR Green PCR kit (Qiagen) on cDNA
780 corresponding to 25 ng of total RNA using the following conditions: 95 ºC for 15 min, and 40
781 cycles at 94 ºC for 15 s, 60 ºC for 30 s and 72 ºC for 30 s. Gene-specific primer pairs were
782 designed using Primer3 software [128]. Dissociation analysis from 55 ºC to 90 ºC of the end
783 product was performed to ensure specificity. Cycle of threshold (CT) values were normalised
784 to the GAPDH reference to calculate the relative level of gene expression on the $\log_2$ scale
785 (ΔCT). Mean ΔCT values from BN rats were then subtracted from each sample ΔCT to obtain
786 ΔΔCT values.

787 **RNA sequencing and analysis**

788 RNA was isolated as described above from the frozen hippocampus, liver, soleus muscle
789 and perirenal adipose tissue samples isolated from SHR-Tti2$^{+/-}$ rats and wild-type SHR-Tti2$^{+/+}$
790 littermates. RNA integrity was confirmed using BioAnalyzer (Agilent Technologies,
791 Germany). Sequencing libraries were prepared using NEBNext® Ultra™ II Directional RNA
792 Library Prep Kit for Illumina® from 300 ng of total RNA, with mRNA enrichment by poly-dT
793 pull down using the NEBNext Poly(A) mRNA Magnetic Isolation Module (NEB) according to
794 the manufacturer's instructions. Samples were then directly subjected to the workflow for
795 strand-specific RNA-Seq library preparation (Ultra II Directional RNA Library Prep, NEB). For
796 ligation custom adaptors were used (Adaptor-Oligo 1: 5'-ACA CTC TTT CCC TAC ACG ACG
797 CTC TTC CGA TCT-3', Adaptor-Oligo 2: 5'-P-GAT CGG AAG AGC ACA CGT CTG AAC
798 TCC AGT CAC-3'). After ligation, adapters were depleted by an XP bead purification
799 (Beckman Coulter) adding the beads solution in a ratio of 1:0.9. Dual indexing was done
800 during the following PCR enrichment (12 cycles, 65 °C) using custom amplification primers

bioRxiv preprint doi: https://doi.org/10.1101/2021.06.04.447058; this version posted June 4, 2021. The copyright holder for this preprint (which was not certified by peer review) is the author/funder, who has granted bioRxiv a license to display the preprint in perpetuity. It is made available under a CC-BY 4.0 International license.

carrying the same sequence for i7 and i5 index (Primer 1: AAT GAT ACG GCG ACC ACC GAG ATC TAC AC NNNNNNNN ACA TCT TTC CCT ACA CGA CGC TCT TCC GAT CT, Primer 2: CAA GCA GAA GAC GGC ATA CGA GAT NNNNNNNN GTG ACT GGA GTT CAG ACG TGT GCT CTT CCG ATC T). After two more XP bead purifications (1:0.9), libraries were quantified using the Fragment Analyzer (Agilent). For Illumina flowcell production, samples were equimolarly pooled and sequenced 75bp single-end on multiple Illumina NextSeq 500 flowcells, aiming for approximately 30 million sequencing reads per sample.

Expression levels of individual transcripts were estimated by kallisto (ver. 0.46.1) [129] using Ensembl cDNA database (release 97) [130] as a reference. The software was executed with sequence-based bias correction, 100 bootstrap samples, an average fragment length of 200 bp and standard deviation set to 20. Differential expression analysis was carried out using an R package sleuth (ver. 0.30.0) [131]. A single outlier hippocampus sample was identified by examining a principal component projection and removed from further analysis. Samples obtained from each tissue were used to fit independent statistical models, with genotype as a single covariate, using 5 or 4 replicates per genotype. Statistical significances of changes in transcript abundances were computed using a Wald test. A 10 % FDR (false discovery rate) cut-off and an absolute value of fold change of 1.5 were used to identify differentially expressed genes. Functional enrichment analysis was performed with Ingenuity Pathway Analysis software (IPA; Qiagen) at default settings [132].

Basal and insulin stimulated glycogen synthesis in skeletal muscle.

For measurement of insulin stimulated incorporation of glucose into glycogen, diaphragmatic muscles were incubated for 2 h in 95% O_2 + 5% CO_2 in Krebs-Ringer bicarbonate buffer, pH 7.4, containing 0.1 µCi/ml of ^{14}C-U glucose, 5 mmol/L of unlabelled glucose, and 2.5 mg/ml of bovine serum albumin (Armour, Fraction V), with or without 250 µU/ml insulin. Glycogen was extracted, and basal and insulin stimulated incorporation of glucose into glycogen was determined.

bioRxiv preprint doi: https://doi.org/10.1101/2021.06.04.447058; this version posted June 4, 2021. The copyright holder for this preprint (which was not certified by peer review) is the author/funder, who has granted bioRxiv a license to display the preprint in perpetuity. It is made available under aCC-BY 4.0 International license.

827 **Glucose utilization in isolated epididymal adipose tissue and brown adipose tissue.**

828 Distal parts of epididymal adipose tissue or interscapular brown adipose tissue were
829 rapidly dissected and incubated for 2 hours in Krebs-Ringer bicarbonate buffer with 5 mmol/L
830 glucose, 0.1 □Ci ^{14}C-U-glucose/mL (UVVR, Prague, Czech Republic) and 2% bovine serum
831 albumin, gaseous phase 95% O_2 and 5% CO_2 in the presence (250 □U/mL) or absence of
832 insulin in incubation media. All incubations were performed at 37 °C in sealed vials in a
833 shaking water bath. Then we estimated incorporation of ^{14}C-glucose into neutral lipids.
834 Briefly, adipose tissue was removed from incubation medium, rinsed in saline, and
835 immediately put into chloroform. The pieces of tissue were dissolved using a Teflon pestle
836 homogenizer, methanol was added (chloroform:methanol 2:1), and lipids were extracted at
837 4 °C overnight. The remaining tissue was removed, KH_2PO_4 was added and a clear extract
838 was taken for further analysis. An aliquot was evaporated, reconstituted in scintillation liquid,
839 and the radioactivity measured by scintillation counting. Incremental glucose utilization was
840 calculated as the difference between the insulin stimulated and basal incorporation of
841 glucose into neutral lipids.

842 **Lipolysis in isolated epididymal adipose tissue.**

843 For measurement of basal and adrenaline stimulated lipolysis, the distal parts of
844 epididymal adipose tissue were incubated in Krebs-Ringer phosphate buffer containing 3 %
845 bovine serum albumin (Armour, Fraction V) at 37 °C, pH 7.4 with or without adrenaline (0.25
846 µg/ml). The tissue was incubated for 2 hours and the concentrations of NEFA and glycerol in
847 the medium were determined.

848 **Tissue triglyceride and cholesterol measurements.**

849 For determination of triglycerides in liver, gastrocnemius muscle, kidney, and heart,
850 tissues were powdered under liquid N_2 and extracted for 16 hours in chloroform:methanol,
851 after which 2 % KH_2PO_4 was added and the solution was centrifuged. The organic phase
852 was removed and evaporated under N_2. The resulting pellet was dissolved in isopropyl

bioRxiv preprint doi: https://doi.org/10.1101/2021.06.04.447058; this version posted June 4, 2021. The copyright holder for this preprint (which was not certified by peer review) is the author/funder, who has granted bioRxiv a license to display the preprint in perpetuity. It is made available under aCC-BY 4.0 International license.

alcohol, and triglyceride and cholesterol concentrations were determined by enzymatic assay (Pliva-Lachema, Brno, Czech Republic).

Biochemical analyses.

Blood glucose levels were measured by the glucose oxidase assay (Pliva-Lachema, Brno, Czech Republic) using tail vein blood drawn into 5 % trichloracetic acid and promptly centrifuged. NEFA levels were determined using an acyl-CoA oxidase-based colorimetric kit (Roche Diagnostics GmbH, Mannheim, Germany). Serum triglyceride and cholesterol concentrations were measured by standard enzymatic methods (Pliva-Lachema, Brno, Czech Republic). Glycerol was determined using an analytical kit from Sigma. Serum insulin concentrations were determined using a rat insulin ELISA kit (Mercodia, Uppsala, Sweden).

Parameters of oxidative stress.

Activities of superoxide dismutase (SOD), glutathione peroxidase (GSH-Px), and glutathione reductase (GR) were analysed using Cayman Chemicals assay kits (MI, USA) according to manufacturer's instructions. Catalase (CAT) activity measurement was based on the ability of H_2O_2 to produce with ammonium molybdate a colour complex detected spectrophotometrically. The level of reduced glutathione (GSH) was determined in the reaction of SH-groups using Ellman reagent. The level of reduced (GSH) and oxidized (GSSG) form of glutathione was determined by high-performance liquid chromatography method with fluorescent detection according to HPLC diagnostic kit (Chromsystems, Munich, Germany). Lipoperoxidation products were assessed by the levels of thiobarbituric acid reactive substances (TBARS) determined by assaying the reaction with thiobarbituric acid. The levels of conjugated dienes were analysed by extraction in the media (heptane:isopropanol = 2:1) and measured spectrophotometrically in heptane's layer.

Statistical analysis

Statistical analyses were performed in R [133]. Normality of distribution of strain means for neurogenesis phenotypes was checked using Shapiro-Wilk test. Differences between groups

bioRxiv preprint doi: https://doi.org/10.1101/2021.06.04.447058; this version posted June 4, 2021. The copyright holder for this preprint (which was not certified by peer review) is the author/funder, who has granted bioRxiv a license to display the preprint in perpetuity. It is made available under a CC-BY 4.0 International license.

were tested using Student's *t*-test or ANOVA followed by Tukey or Dunnett's post hoc test. Responses to insulin were analysed with a two-way linear mixed effect models using the lme4 R package [120]. Genotype, insulin treatment and interaction between genotype and treatment were used as fixed effects and individual intercepts were used as a random effect. Significance of main terms was evaluated by likelihood ratio test using function *Anova* from the car package [134], followed by Tukey post hoc test using multcomp package [135]. Values are represented as means +/- standard error of the mean. Plots were generated using the ggplot2 package [136].

Data

Neurogenesis data was deposited in the HXB/BXH Published Phenotypes Database at the GeneNetwork (www.genenetwork.org) under Record IDs: 10193 ($BrdU^+$ cells), 10194 ($Ki67^+$ cells), 10195 (clusters of $Ki67^+$ cells). Hippocampal gene expression dataset was deposited at GeneNetwork under GN Accession GN231. RNA sequencing of SHR and SHR-$Tti2^{+/-}$ rats was deposited to Gene Ontology Omnibus under the accession number GSE160361.

bioRxiv preprint doi: https://doi.org/10.1101/2021.06.04.447058; this version posted June 4, 2021. The copyright holder for this preprint (which was not certified by peer review) is the author/funder, who has granted bioRxiv a license to display the preprint in perpetuity. It is made available under a CC-BY 4.0 International license.

References

1. Panza F, Solfrizzi V, Logroscino G, Maggi S, Santamato A, Seripa D, et al. Current epidemiological approaches to the metabolic-cognitive syndrome. Journal of Alzheimer's Disease. IOS Press; 2012. doi:10.3233/JAD-2012-111496
2. Watanabe K, Stringer S, Frei O, Umićević Mirkov M, de Leeuw C, Polderman TJC, et al. A global overview of pleiotropy and genetic architecture in complex traits. Nat Genet. 2019;51: 1339–1348. doi:10.1038/s41588-019-0481-0
3. Lumsden AL, Mulugeta A, Zhou A, Hyppönen E. Apolipoprotein E (APOE) genotype-associated disease risks: a phenome-wide, registry-based, case-control study utilising the UK Biobank. EBioMedicine. 2020;59. doi:10.1016/j.ebiom.2020.102954
4. Nikpay M, Mohammadzadeh S. Phenome-wide screening for traits causally associated with the risk of coronary artery disease. J Hum Genet. 2020;65: 371–380. doi:10.1038/s10038-019-0716-z
5. Andreassen OA, Djurovic S, Thompson WK, Schork AJ, Kendler KS, O'Donovan MC, et al. Improved detection of common variants associated with schizophrenia by leveraging pleiotropy with cardiovascular-disease risk factors. Am J Hum Genet. 2013;92: 197–209. doi:10.1016/j.ajhg.2013.01.001
6. Zhang T, Goodman M, Zhu F, Healy B, Carruthers R, Chitnis T, et al. Phenome-wide examination of comorbidity burden and multiple sclerosis disease severity. Neurol Neuroimmunol neuroinflammation. 2020;7. doi:10.1212/NXI.0000000000000864
7. Thomassen JQ, Tolstrup JS, Benn M, Frikke-Schmidt R. Type-2 diabetes and risk of dementia: Observational and Mendelian randomisation studies in 1 million individuals. Epidemiol Psychiatr Sci. 2020;29. doi:10.1017/S2045796020000347
8. Mollon J, Curran JE, Mathias SR, Knowles EEM, Carlisle P, Fox PT, et al. Neurocognitive impairment in type 2 diabetes: evidence for shared genetic aetiology. Diabetologia. 2020;63: 977–986. doi:10.1007/s00125-020-05101-y
9. Stearns FW. One hundred years of pleiotropy: A retrospective. Genetics. Genetics; 2010. pp. 767–773. doi:10.1534/genetics.110.122549
10. Geiler-Samerotte KA, Li S, Lazaris C, Taylor A, Ziv N, Ramjeawan C, et al. Extent and context dependence of pleiotropy revealed by high-throughput single-cell phenotyping. PLoS Biol. 2020;18. doi:10.1371/journal.pbio.3000836
11. White JK, Gerdin AK, Karp NA, Ryder E, Buljan M, Bussell JN, et al. XGenome-wide generation and systematic phenotyping of knockout mice reveals new roles for many genes. Cell. 2013;154: 452. doi:10.1016/j.cell.2013.06.022
12. McGuigan K, Collet JM, McGraw EA, Ye YH, Allen SL, Chenoweth SF, et al. The nature and extent of mutational pleiotropy in gene expression of male Drosophila serrata. Genetics. 2014;196: 911–921. doi:10.1534/genetics.114.161232
13. Wagner GP, Zhang J. The pleiotropic structure of the genotype-phenotype map: The evolvability of complex organisms. Nature Reviews Genetics. Nat Rev Genet; 2011. pp. 204–213. doi:10.1038/nrg2949
14. Sivakumaran S, Agakov F, Theodoratou E, Prendergast JG, Zgaga L, Manolio T, et al. Abundant pleiotropy in human complex diseases and traits. Am J Hum Genet. 2011;89: 607–618. doi:10.1016/j.ajhg.2011.10.004
15. Pickrell JK, Berisa T, Liu JZ, Ségurel L, Tung JY, Hinds DA. Detection and interpretation of shared genetic influences on 42 human traits. Nat Genet. 2016;48: 709–717. doi:10.1038/ng.3570
16. Shikov AE, Skitchenko RK, Predeus A V., Barbitoff YA. Phenome-wide functional dissection of pleiotropic effects highlights key molecular pathways for human complex traits. Sci Rep. 2020;10: 1–10. doi:10.1038/s41598-020-58040-4
17. Jordan DM, Verbanck M, Do R. HOPS: A quantitative score reveals pervasive horizontal pleiotropy in human genetic variation is driven by extreme polygenicity of human traits and diseases. Genome Biol. 2019;20. doi:10.1186/s13059-019-1844-7
18. Toda T, Gage FH. Review: adult neurogenesis contributes to hippocampal plasticity.

bioRxiv preprint doi: https://doi.org/10.1101/2021.06.04.447058; this version posted June 4, 2021. The copyright holder for this preprint (which was not certified by peer review) is the author/funder, who has granted bioRxiv a license to display the preprint in perpetuity. It is made available under aCC-BY 4.0 International license.

Cell and Tissue Research. Springer Verlag; 2018. pp. 693–709. doi:10.1007/s00441-017-2735-4

19. Spalding KL, Bergmann O, Alkass K, Bernard S, Salehpour M, Huttner HB, et al. XDynamics of hippocampal neurogenesis in adult humans. Cell. 2013;153: 1219. doi:10.1016/j.cell.2013.05.002
20. Knobloch M, Jessberger S. Metabolism and neurogenesis. Current Opinion in Neurobiology. Elsevier Ltd; 2017. pp. 45–52. doi:10.1016/j.conb.2016.11.006
21. Kempermann G, Chesler EJ, Lu L, Williams RW, Gage FH. Natural variation and genetic covariance in adult hippocampal neurogenesis. Proc Natl Acad Sci U S A. 2006;103: 780–785. doi:10.1073/pnas.0510291103
22. Kempermann G, Kuhn HG, Gage FH. Genetic influence on neurogenesis in the dentate gyrus of adult mice. Proc Natl Acad Sci U S A. 1997;94: 10409–10414. doi:10.1073/pnas.94.19.10409
23. Printz MP, Jirout M, Jaworski R, Alemayehu A, Kren V. Invited review: HXB/BXH rat recombinant inbred strain platform: A newly enhanced tool for cardiovascular, behavioral, and developmental genetics and genomics. Journal of Applied Physiology. American Physiological Society; 2003. pp. 2510–2522. doi:10.1152/japplphysiol.00064.2003
24. Liska F, Peterkovaa R, Peterka M, Landa V, Zõadek V, Mlejnek P, et al. Targeting of the Plzf gene in the rat by transcription activator-like Effector nuclease results in caudal regression syndrome in spontaneously hypertensive rats. PLoS One. 2016;11. doi:10.1371/journal.pone.0164206
25. Mondon CE, Reaven GM. Evidence of abnormalities of insulin metabolism in rats with spontaneous hypertension. Metabolism. 1988;37: 303–305. doi:10.1016/0026-0495(88)90127-8
26. Pravenec M, Zídek V, Landa V, Šimáková M, Mlejnek P, Kazdová L, et al. Genetic Analysis of “Metabolic Syndrome” in the Spontaneously Hypertensive Rat. Physiol Res. 2004;53: 15–22. Available: http://www.biomed.cas.cz/physiolres
27. Pravenec M. Use of rat genomics for investigating the metabolic syndrome. Methods Mol Biol. 2010;597: 415–426. doi:10.1007/978-1-60327-389-3_28
28. Terry A V., Hernandez CM, Buccafusco JJ, Gattu M. Deficits in spatial learning and nicotinic-acetylcholine receptors in older, spontaneously hypertensive rats. Neuroscience. 2000;101: 357–368. doi:10.1016/S0306-4522(00)00377-8
29. Grünblatt E, Bartl J, Iuhos D-I, Knezovic A, Trkulja V, Riederer P, et al. Characterization of cognitive deficits in spontaneously hypertensive rats, accompanied by brain insulin receptor dysfunction. J Mol Psychiatry. 2015;3. doi:10.1186/s40303-015-0012-6
30. Sabbatini M, Strocchi P, Vitaioli L, Amenta F. The hippocampus in spontaneously hypertensive rats: A quantitative microanatomical study. Neuroscience. 2000;100: 251–258. doi:10.1016/S0306-4522(00)00297-9
31. Mignini F, Vitaioli L, Sabbatini M, Tomassoni D, Amenta F. The cerebral cortex of spontaneously hypertensive rats: A quantitative microanatomical study. Clinical and Experimental Hypertension. Clin Exp Hypertens; 2004. pp. 287–303. doi:10.1081/CEH-120034135
32. Tabakoff B, Smith H, Vanderlinden LA, Hoffman PL, Saba LM. Networking in Biology: The Hybrid Rat Diversity Panel. Methods in Molecular Biology. Humana Press Inc.; 2019. pp. 213–231. doi:10.1007/978-1-4939-9581-3_10
33. Wilkinson MD, Dumontier M, Aalbersberg IjJ, Appleton G, Axton M, Baak A, et al. Comment: The FAIR Guiding Principles for scientific data management and stewardship. Sci Data. 2016;3: 1–9. doi:10.1038/sdata.2016.18
34. Mulligan MK, Mozhui K, Prins P, Williams RW. Genenetwork: A toolbox for systems genetics. Methods in Molecular Biology. Humana Press Inc.; 2017. pp. 75–120. doi:10.1007/978-1-4939-6427-7_4
35. Aitman TJ, Critser JK, Cuppen E, Dominiczak A, Fernandez-Suarez XM, Flint J, et al. Progress and prospects in rat genetics: A community view. Nature Genetics. Nat

bioRxiv preprint doi: https://doi.org/10.1101/2021.06.04.447058; this version posted June 4, 2021. The copyright holder for this preprint (which was not certified by peer review) is the author/funder, who has granted bioRxiv a license to display the preprint in perpetuity. It is made available under aCC-BY 4.0 International license.

Genet; 2008. pp. 516–522. doi:10.1038/ng.147

36. Morrissey C, Grieve IC, Heinig M, Atanur S, Petretto E, Pravenec M, et al. Integrated genomic approaches to identification of candidate genes underlying metabolic and cardiovascular phenotypes in the spontaneously hypertensive rat. Physiol Genomics. 2011;43: 1207–1218. doi:10.1152/physiolgenomics.00210.2010
37. Hubner N, Wallace CA, Zimdahl H, Petretto E, Schulz H, Maciver F, et al. Integrated transcriptional profiling and linkage analysis for identification of genes underlying disease. Nat Genet. 2005;37: 243–253. doi:10.1038/ng1522
38. Petretto E, Mangion J, Dickens NJ, Cook SA, Kumaran MK, Lu H, et al. Heritability and tissue specificity of expression quantitative trait loci. PLoS Genet. 2006;2: 1625–1633. doi:10.1371/journal.pgen.0020172
39. Adriaens ME, Lodder EM, Moreno-Moral A, Silhavý J, Heinig M, Glinge C, et al. Systems genetics approaches in rat identify novel genes and gene networks associated with cardiac conduction. J Am Heart Assoc. 2018;7. doi:10.1161/JAHA.118.009243
40. Heinig M, Petretto E, Wallace C, Bottolo L, Rotival M, Lu H, et al. A trans-acting locus regulates an anti-viral expression network and type 1 diabetes risk. Nature. 2010;467: 460–464. doi:10.1038/nature09386
41. Pravenec M, Churchill PC, Churchill MC, Viklicky O, Kazdova L, Aitman TJ, et al. Identification of renal Cd36 as a determinant of blood pressure and risk for hypertension. Nat Genet. 2008;40: 952–954. doi:10.1038/ng.164
42. Atanur SS, Birol I, Guryev V, Hirst M, Hummel O, Morrissey C, et al. The genome sequence of the spontaneously hypertensive rat: Analysis and functional significance. Genome Res. 2010;20: 791–803. doi:10.1101/gr.103499.109
43. Simonis M, Atanur SS, Linsen S, Guryev V, Ruzius FP, Game L, et al. Genetic basis of transcriptome differences between the founder strains of the rat HXB/BXH recombinant inbred panel. Genome Biol. 2012;13. doi:10.1186/gb-2012-13-4-r31
44. Nadeau JH, Burrage LC, Restivo J, Pao YH, Churchill G, Hoit BD. Pleiotropy, homeostasis, and functional networks based on assays of cardiovascular traits in genetically randomized populations. Genome Res. 2003;13: 2082–2091. doi:10.1101/gr.1186603
45. Kempermann G, Gast D, Kronenberg G, Yamaguchi M, Gage FH. Early determination and long-term persistence of adult-generated new neurons in the hippocampus of mice. Development. Development; 2003. pp. 391–399. doi:10.1242/dev.00203
46. Zocher S, Schilling S, Grzyb AN, Adusumilli VS, Lopes JB, Günther S, et al. Early-life environmental enrichment generates persistent individualized behavior in mice. Sci Adv. 2020;6. doi:10.1126/sciadv.abb1478
47. Li R, Tsaih SW, Shockley K, Stylianou IM, Wergedal J, Paigen B, et al. Structural model analysis of multiple quantitative traits. PLoS Genet. 2006;2: 1046–1057. doi:10.1371/journal.pgen.0020114
48. Leduc MS, Blair RH, Verdugo RA, Tsaih SW, Walsh K, Churchill GA, et al. Using bioinformatics and systems genetics to dissect HDL-cholesterol genetics in an MRL/MpJ x SM/J intercross. J Lipid Res. 2012;53: 1163–1175. doi:10.1194/jlr.M025833
49. Leduc MS, Hageman RS, Verdugo RA, Tsaih SW, Walsh K, Churchill GA, et al. Integration of QTL and bioinformatic tools to identify candidate genes for triglycerides in mice. J Lipid Res. 2011;52: 1672–1682. doi:10.1194/jlr.M011130
50. Sugimoto K. Branching the Tel2 pathway for exact fit on phosphatidylinositol 3-kinase-related kinases. Current Genetics. Springer Verlag; 2018. pp. 965–970. doi:10.1007/s00294-018-0817-9
51. Ardlie KG, DeLuca DS, Segrè A V., Sullivan TJ, Young TR, Gelfand ET, et al. The Genotype-Tissue Expression (GTEx) pilot analysis: Multitissue gene regulation in humans. Science (80-). 2015;348: 648–660. doi:10.1126/science.1262110
52. Nicolae DL, Gamazon E, Zhang W, Duan S, Dolan ME, Cox NJ. Trait-Associated SNPs Are More Likely to Be eQTLs: Annotation to Enhance Discovery from GWAS.

bioRxiv preprint doi: https://doi.org/10.1101/2021.06.04.447058; this version posted June 4, 2021. The copyright holder for this preprint (which was not certified by peer review) is the author/funder, who has granted bioRxiv a license to display the preprint in perpetuity. It is made available under aCC-BY 4.0 International license.

Gibson G, editor. PLoS Genet. 2010;6: e1000888. doi:10.1371/journal.pgen.1000888
53. Hurov KE, Cotta-Ramusino C, Elledge SJ. A genetic screen identifies the Triple T complex required for DNA damage signaling and ATM and ATR stability. Genes Dev. 2010;24: 1939–1950. doi:10.1101/gad.1934210
54. Hořejší Z, Takai H, Adelman CA, Collis SJ, Flynn H, Maslen S, et al. CK2 phospho-dependent binding of R2TP complex to TEL2 is essential for mTOR and SMG1 stability. Mol Cell. 2010;39: 839–850. doi:10.1016/j.molcel.2010.08.037
55. Takai H, Xie Y, De Lange T, Pavletich NP. Tel2 structure and function in the Hsp90-dependent maturation of mTOR and ATR complexes. Genes Dev. 2010;24: 2019–2030. doi:10.1101/gad.1956410
56. Stirling PC, Bloom MS, Solanki-Patil T, Smith S, Sipahimalani P, Li Z, et al. The complete spectrum of yeast chromosome instability genes identifies candidate cin cancer genes and functional roles for astra complex components. PLoS Genet. 2011;7. doi:10.1371/journal.pgen.1002057
57. Takai H, Wang RC, Takai KK, Yang H, de Lange T. Tel2 Regulates the Stability of PI3K-Related Protein Kinases. Cell. 2007;131: 1248–1259. doi:10.1016/j.cell.2007.10.052
58. Kaizuka T, Hara T, Oshiro N, Kikkawa U, Yonezawa K, Takehana K, et al. Tti1 and Tel2 are critical factors in mammalian target of rapamycin complex assembly. J Biol Chem. 2010;285: 20109–20116. doi:10.1074/jbc.M110.121699
59. Yamashita A. Role of SMG-1-mediated Upf1 phosphorylation in mammalian nonsense-mediated mRNA decay. Genes to Cells. Genes Cells; 2013. pp. 161–175. doi:10.1111/gtc.12033
60. Cimprich KA, Cortez D. ATR: An essential regulator of genome integrity. Nature Reviews Molecular Cell Biology. Nat Rev Mol Cell Biol; 2008. pp. 616–627. doi:10.1038/nrm2450
61. Shimobayashi M, Hall MN. Making new contacts: The mTOR network in metabolism and signalling crosstalk. Nat Rev Mol Cell Biol. 2014;15: 155–162. doi:10.1038/nrm3757
62. Murr R, Vaissière T, Sawan C, Shukla V, Herceg Z. Orchestration of chromatin-based processes: Mind the TRRAP. Oncogene. Oncogene; 2007. pp. 5358–5372. doi:10.1038/sj.onc.1210605
63. Abraham RT. PI 3-kinase related kinases: “Big” players in stress-induced signaling pathways. DNA Repair. Elsevier; 2004. pp. 883–887. doi:10.1016/j.dnarep.2004.04.002
64. Hoffman KS, Duennwald ML, Karagiannis J, Genereaux J, McCarton AS, Brandl CJ. Saccharomyces cerevisiae Tti2 regulates PIKK proteins and stress response. G3 Genes, Genomes, Genet. 2016;6: 1649–1659. doi:10.1534/g3.116.029520
65. Garcia N, Messing J. TTT and PIKK complex genes reverted to single copy following polyploidization and retain function despite massive retrotransposition in maize. Front Plant Sci. 2017;8. doi:10.3389/fpls.2017.01723
66. Petersen MC, Shulman GI. Mechanisms of insulin action and insulin resistance. Physiological Reviews. American Physiological Society; 2018. pp. 2133–2223. doi:10.1152/physrev.00063.2017
67. Shan T, Zhang P, Jiang Q, Xiong Y, Wang Y, Kuang S. Adipocyte-specific deletion of mTOR inhibits adipose tissue development and causes insulin resistance in mice. Diabetologia. 2016;59: 1995–2004. doi:10.1007/s00125-016-4006-4
68. Kumar A, Harris TE, Keller SR, Choi KM, Magnuson MA, Lawrence JC. Muscle-Specific Deletion of Rictor Impairs Insulin-Stimulated Glucose Transport and Enhances Basal Glycogen Synthase Activity. Mol Cell Biol. 2008;28: 61–70. doi:10.1128/mcb.01405-07
69. Kumar A, Lawrence JC, Jung DY, Ko HJ, Keller SR, Kim JK, et al. Fat cell-specific ablation of rictor in mice impairs insulin-regulated fat cell and whole-body glucose and lipid metabolism. Diabetes. 2010;59: 1397–1406. doi:10.2337/db09-1061
70. Takagi M, Uno H, Nishi R, Sugimoto M, Hasegawa S, Piao J, et al. ATM Regulates

bioRxiv preprint doi: https://doi.org/10.1101/2021.06.04.447058; this version posted June 4, 2021. The copyright holder for this preprint (which was not certified by peer review) is the author/funder, who has granted bioRxiv a license to display the preprint in perpetuity. It is made available under aCC-BY 4.0 International license.

Adipocyte Differentiation and Contributes to Glucose Homeostasis. Cell Rep. 2015;10: 957–967. doi:10.1016/j.celrep.2015.01.027

71. Mao Z, Zhang W. Role of mTOR in glucose and lipid metabolism. International Journal of Molecular Sciences. MDPI AG; 2018. doi:10.3390/ijms19072043
72. Langouët M, Saadi A, Rieunier G, Moutton S, Siquier-Pernet K, Fernet M, et al. Mutation in TTI2 reveals a role for triple T complex in human brain development. Hum Mutat. 2013;34: 1472–1476. doi:10.1002/humu.22399
73. Mainardi M, Fusco S, Grassi C. Modulation of hippocampal neural plasticity by glucose-related signaling. Neural Plasticity. Hindawi Publishing Corporation; 2015. doi:10.1155/2015/657928
74. Fernandez AM, Torres-Alemán I. The many faces of insulin-like peptide signalling in the brain. Nature Reviews Neuroscience. Nat Rev Neurosci; 2012. pp. 225–239. doi:10.1038/nrn3209
75. van Praag X, Fleshner M, Schwartz MW, Mattson MP. Exercise, energy intake, glucose homeostasis, and the brain. J Neurosci. 2014;34: 15139–15149. doi:10.1523/JNEUROSCI.2814-14.2014
76. Rafalski VA, Brunet A. Energy metabolism in adult neural stem cell fate. Progress in Neurobiology. Prog Neurobiol; 2011. pp. 182–203. doi:10.1016/j.pneurobio.2010.10.007
77. Marissal-Arvy N, Campas MN, Semont A, Ducroix-Crepy C, Beauvieux MC, Brossaud J, et al. Insulin treatment partially prevents cognitive and hippocampal alterations as well as glucocorticoid dysregulation in early-onset insulin-deficient diabetic rats. Psychoneuroendocrinology. 2018;93: 72–81. doi:10.1016/j.psyneuen.2018.04.016
78. Sun P, Knezovic A, Parlak M, Cuber J, Karabeg M, Deckert J, et al. Long-Term Effects of Intracerebroventricular Streptozotocin Treatment on Adult Neurogenesis in the Rat Hippocampus. Curr Alzheimer Res. 2015;12: 772–784. doi:10.2174/1567205012666150710112147
79. Stranahan AM, Arumugam T V., Cutler RG, Lee K, Egan JM, Mattson MP. Diabetes impairs hippocampal function through glucocorticoid-mediated effects on new and mature neurons. Nat Neurosci. 2008;11: 309–317. doi:10.1038/nn2055
80. Zhang WJ, Tan YF, Yue JTY, Vranic M, Wojtowicz JM. Impairment of hippocampal neurogenesis in streptozotocin-treated diabetic rats. Acta Neurol Scand. 2008;117: 205–210. doi:10.1111/j.1600-0404.2007.00928.x
81. Lee J, Seroogy KB, Mattson MP. Dietary restriction enhances neurotrophin expression and neurogenesis in the hippocampus of adult mice. J Neurochem. 2002;80: 539–547. doi:10.1046/j.0022-3042.2001.00747.x
82. Park HR, Park M, Choi J, Park KY, Chung HY, Lee J. A high-fat diet impairs neurogenesis: Involvement of lipid peroxidation and brain-derived neurotrophic factor. Neurosci Lett. 2010;482: 235–239. doi:10.1016/j.neulet.2010.07.046
83. Klein C, Jonas W, Iggena D, Empl L, Rivalan M, Wiedmer P, et al. Exercise prevents high-fat diet-induced impairment of flexible memory expression in the water maze and modulates adult hippocampal neurogenesis in mice. Neurobiol Learn Mem. 2016;131: 26–35. doi:10.1016/j.nlm.2016.03.002
84. Ziegler A, Bader P, McWalter K, Douglas G, Houdayer C, Bris C, et al. Confirmation that variants in TTI2 are responsible for autosomal recessive intellectual disability. Clin Genet. 2019;96: 354–358. doi:10.1111/cge.13603
85. Wang R, Han S, Liu H, Khan A, Xiaerbati H, Yu X, et al. Novel compound heterozygous mutations in tti2 cause syndromic intellectual disability in a chinese family. Front Genet. 2019;10. doi:10.3389/fgene.2019.01060
86. Picher-Martel V, Labrie Y, Rivest S, Lace B, Chrestian N. Whole-exome sequencing identifies homozygous mutation in TTI2 in a child with primary microcephaly: A case report. BMC Neurol. 2020;20. doi:10.1186/s12883-020-01643-1
87. You J, Sobreira NL, Gable DL, Jurgens J, Grange DK, Belnap N, et al. A Syndromic Intellectual Disability Disorder Caused by Variants in TELO2, a Gene Encoding a Component of the TTT Complex. Am J Hum Genet. 2016;98: 909–918.

bioRxiv preprint doi: https://doi.org/10.1101/2021.06.04.447058; this version posted June 4, 2021. The copyright holder for this preprint (which was not certified by peer review) is the author/funder, who has granted bioRxiv a license to display the preprint in perpetuity. It is made available under aCC-BY 4.0 International license.

doi:10.1016/j.ajhg.2016.03.014

88. Moosa S, Altmüller J, Lyngbye T, Christensen R, Li Y, Nürnberg P, et al. Novel compound heterozygous mutations in TELO2 in a patient with severe expression of You-Hoover-Fong syndrome. Mol Genet Genomic Med. 2017;5: 580–584. doi:10.1002/mgg3.287
89. Choy KR, Watters DJ. Neurodegeneration in ataxia-telangiectasia: Multiple roles of ATM kinase in cellular homeostasis. Developmental Dynamics. John Wiley and Sons Inc.; 2018. pp. 33–46. doi:10.1002/dvdy.24522
90. Shiloh Y, Ziv Y. The ATM protein kinase: Regulating the cellular response to genotoxic stress, and more. Nature Reviews Molecular Cell Biology. Nat Rev Mol Cell Biol; 2013. pp. 197–210. doi:10.1038/nrm3546
91. O'Driscoll M, Ruiz-Perez VL, Woods CG, Jeggo PA, Goodship JA. A splicing mutation affecting expression of ataxia-telangiectasia and Rad3-related protein (ATR) results in Seckel syndrome. Nat Genet. 2003;33: 497–501. doi:10.1038/ng1129
92. Branzei D, Foiani M. Regulation of DNA repair throughout the cell cycle. Nature Reviews Molecular Cell Biology. Nature Publishing Group; 2008. pp. 297–308. doi:10.1038/nrm2351
93. Enriquez-Rios V, Dumitrache LC, Downing SM, Li Y, Brown EJ, Russell HR, et al. DNA-PKcs, ATM, and ATR interplay maintains genome integrity during neurogenesis. J Neurosci. 2017;37: 893–905. doi:10.1523/JNEUROSCI.4213-15.2016
94. Allen DM, Van Praag H, Ray J, Weaver Z, Winrow CJ, Carter TA, et al. Ataxia telangiectasia mutated is essential during adult neurogenesis. Genes Dev. 2001;15: 554–566. doi:10.1101/gad.869001
95. Lee Y, Shull ERP, Frappart PO, Katyal S, Enriquez-Rios V, Zhao J, et al. ATR maintains select progenitors during nervous system development. EMBO J. 2012;31: 1177–1189. doi:10.1038/emboj.2011.493
96. Coufal NG, Garcia-Perez JL, Peng GE, Marchetto MCN, Muotri AR, Mu Y, et al. Ataxia telangiectasia mutated (ATM) modulates long interspersed element-1 (L1) retrotransposition in human neural stem cells. Proc Natl Acad Sci U S A. 2011;108: 20382–20387. doi:10.1073/pnas.1100273108
97. Singer T, McConnell MJ, Marchetto MCN, Coufal NG, Gage FH. LINE-1 retrotransposons: Mediators of somatic variation in neuronal genomes? Trends Neurosci. 2010;33: 345–354. doi:10.1016/j.tins.2010.04.001
98. Garza-Lombó C, Gonsebatt ME. Mammalian target of rapamycin: Its role in early neural development and in adult and aged brain function. Frontiers in Cellular Neuroscience. Frontiers Media S.A.; 2016. doi:10.3389/fncel.2016.00157
99. Ka M, Condorelli G, Woodgett JR, Kim WY. mTOR regulates brain morphogenesis by mediating GSK3 signaling. Dev. 2014;141: 4076–4086. doi:10.1242/dev.108282
100. Hartman NW, Lin T V., Zhang L, Paquelet GE, Feliciano DM, Bordey A. MTORC1 Targets the Translational Repressor 4E-BP2, but Not S6 Kinase 1/2, to Regulate Neural Stem Cell Self-Renewal InVivo. Cell Rep. 2013;5: 433–444. doi:10.1016/j.celrep.2013.09.017
101. Raman L, Kong X, Kernie SG. Pharmacological inhibition of the mTOR pathway impairs hippocampal development in mice. Neurosci Lett. 2013;541: 9–14. doi:10.1016/j.neulet.2013.01.045
102. Åberg MAI, Åberg ND, Palmer TD, Alborn AM, Carlsson-Skwirut C, Bang P, et al. IGF-I has a direct proliferative effect in adult hippocampal progenitor cells. Mol Cell Neurosci. 2003;24: 23–40. doi:10.1016/S1044-7431(03)00082-4
103. Trejo JL, Carro E, Torres-Alemán I. Circulating insulin-like growth factor I mediates exercise-induced increases in the number of new neurons in the adult hippocampus. J Neurosci. 2001;21: 1628–1634. doi:10.1523/jneurosci.21-05-01628.2001
104. Lichtenwalner RJ, Forbes ME, Bennett SA, Lynch CD, Sonntag WE, Riddle DR. Intracerebroventricular infusion of insulin-like growth factor-I ameliorates the age-related decline in hippocampal neurogenesis. Neuroscience. 2001;107: 603–613. doi:10.1016/S0306-4522(01)00378-5

bioRxiv preprint doi: https://doi.org/10.1101/2021.06.04.447058; this version posted June 4, 2021. The copyright holder for this preprint (which was not certified by peer review) is the author/funder, who has granted bioRxiv a license to display the preprint in perpetuity. It is made available under aCC-BY 4.0 International license.

105. Cheng CM, Cohen M, Tseng V, Bondy CA. Endogenous IGF1 enhances cell survival in the postnatal dentate gyrus. J Neurosci Res. 2001;64: 341–347. doi:10.1002/jnr.1084
106. Agis-Balboa RC, Fischer A. Generating new neurons to circumvent your fears: The role of IGF signaling. Cellular and Molecular Life Sciences. Cell Mol Life Sci; 2014. pp. 21–42. doi:10.1007/s00018-013-1316-2
107. Chaker Z, Aïd S, Berry H, Holzenberger M. Suppression of IGF-I signals in neural stem cells enhances neurogenesis and olfactory function during aging. Aging Cell. 2015;14: 847–856. doi:10.1111/acel.12365
108. Kuwabara T, Kagalwala MN, Onuma Y, Ito Y, Warashina M, Terashima K, et al. Insulin biosynthesis in neuronal progenitors derived from adult hippocampus and the olfactory bulb. EMBO Mol Med. 2011;3: 742–754. doi:10.1002/emmm.201100177
109. Van Brocklyn JR, Williams JB. The control of the balance between ceramide and sphingosine-1-phosphate by sphingosine kinase: Oxidative stress and the seesaw of cell survival and death. Comparative Biochemistry and Physiology - B Biochemistry and Molecular Biology. Elsevier Inc.; 2012. pp. 26–36. doi:10.1016/j.cbpb.2012.05.006
110. Ghasemi R, Dargahi L, Ahmadiani A. Integrated sphingosine-1 phosphate signaling in the central nervous system: From physiological equilibrium to pathological damage. Pharmacological Research. Academic Press; 2016. pp. 156–164. doi:10.1016/j.phrs.2015.11.006
111. Karunakaran I, van Echten-Deckert G. Sphingosine 1-phosphate – A double edged sword in the brain. Biochimica et Biophysica Acta - Biomembranes. Elsevier B.V.; 2017. pp. 1573–1582. doi:10.1016/j.bbamem.2017.03.008
112. Kanno T, Nishizaki T, Proia RL, Kajimoto T, Jahangeer S, Okada T, et al. Regulation of synaptic strength by sphingosine 1-phosphate in the hippocampus. Neuroscience. 2010;171: 973–980. doi:10.1016/j.neuroscience.2010.10.021
113. Martin JL, Lin MZ, McGowan EM, Baxter RC. Potentiation of growth factor signaling by insulin-like growth factor-binding protein-3 in breast epithelial cells requires sphingosine kinase activity. J Biol Chem. 2009;284: 25542–25552. doi:10.1074/jbc.M109.007120
114. Jęśko H, Stępień A, Lukiw WJ, Strosznajder RP. The Cross-Talk Between Sphingolipids and Insulin-Like Growth Factor Signaling: Significance for Aging and Neurodegeneration. Molecular Neurobiology. Humana Press Inc.; 2019. pp. 3501–3521. doi:10.1007/s12035-018-1286-3
115. Paliouras GN, Hamilton LK, Aumont A, Joppé SE, Barnab́-Heider F, Fernandes KJL. Mammalian target of rapamycin signaling is a key regulator of the transit-amplifying progenitor pool in the adult and aging forebrain. J Neurosci. 2012;32: 15012–15026. doi:10.1523/JNEUROSCI.2248-12.2012
116. Sandberg R, Larsson O. Improved precision and accuracy for microarrays using updated probe set definitions. BMC Bioinformatics. 2007;8. doi:10.1186/1471-2105-8-48
117. Irizarry RA, Hobbs B, Collin F, Beazer-Barclay YD, Antonellis KJ, Scherf U, et al. Exploration, normalization, and summaries of high density oligonucleotide array probe level data. Biostatistics. 2003;4: 249–264. doi:10.1093/biostatistics/4.2.249
118. Gautier L, Cope L, Bolstad BM, Irizarry RA. Affy - Analysis of Affymetrix GeneChip data at the probe level. Bioinformatics. 2004;20: 307–315. doi:10.1093/bioinformatics/btg405
119. Mhyre TR, Chesler EJ, Thiruchelvam M, Lungu C, Cory-Slechta DA, Fry JD, et al. Heritability, correlations and in silico mapping of locomotor behavior and neurochemistry in inbred strains of mice. Genes, Brain Behav. 2005;4: 209–228. doi:10.1111/j.1601-183X.2004.00102.x
120. Bates D, Mächler M, Bolker BM, Walker SC. Fitting linear mixed-effects models using lme4. J Stat Softw. 2015;67: 1–48. doi:10.18637/jss.v067.i01
121. Saar K, Beck A, Bihoreau MT, Birney E, Brocklebank D, Chen Y, et al. SNP and haplotype mapping for genetic analysis in the rat. Nat Genet. 2008;40: 560–566.

bioRxiv preprint doi: https://doi.org/10.1101/2021.06.04.447058; this version posted June 4, 2021. The copyright holder for this preprint (which was not certified by peer review) is the author/funder, who has granted bioRxiv a license to display the preprint in perpetuity. It is made available under aCC-BY 4.0 International license.

doi:10.1038/ng.124
122. Wang J, Williams RW, Manly KF. WebQTL: Web-Based Complex Trait Analysis. Neuroinformatics. Neuroinformatics; 2003. pp. 299–308. doi:10.1385/NI:1:4:299
123. Abiola O, Angel JM, Avner P, Bachmanov AA, Belknap JK, Bennett B, et al. The nature and identification of quantitative trait loci: A community's view. Nature Reviews Genetics. Nat Rev Genet; 2003. pp. 911–916. doi:10.1038/nrg1206
124. Lander E, Kruglyak L. Genetic dissection of complex traits: Guidelines for interpreting and reporting linkage results. Nat Genet. 1995;11: 241–247. doi:10.1038/ng1195-241
125. Broman KW, Sen S. A guide to QTL mapping with R/qtl. 2009.
126. Langfelder P, Horvath S. WGCNA: An R package for weighted correlation network analysis. BMC Bioinformatics. 2008;9: 559. doi:10.1186/1471-2105-9-559
127. Smith JR, Hayman GT, Wang SJ, Laulederkind SJF, Hoffman MJ, Kaldunski ML, et al. The Year of the Rat: The Rat Genome Database at 20: A multi-species knowledgebase and analysis platform. Nucleic Acids Res. 2020;48: D731–D742. doi:10.1093/nar/gkz1041
128. Untergasser A, Cutcutache I, Koressaar T, Ye J, Faircloth BC, Remm M, et al. Primer3-new capabilities and interfaces. Nucleic Acids Res. 2012;40: e115. doi:10.1093/nar/gks596
129. Bray NL, Pimentel H, Melsted P, Pachter L. Near-optimal probabilistic RNA-seq quantification. Nat Biotechnol. 2016;34: 525–527. doi:10.1038/nbt.3519
130. Cunningham F, Achuthan P, Akanni W, Allen J, Amode MR, Armean IM, et al. Ensembl 2019. Nucleic Acids Res. 2019;47: D745–D751. doi:10.1093/nar/gky1113
131. Pimentel H, Bray NL, Puente S, Melsted P, Pachter L. Differential analysis of RNA-seq incorporating quantification uncertainty. Nat Methods. 2017;14: 687–690. doi:10.1038/nmeth.4324
132. Krämer A, Green J, Pollard J, Tugendreich S. Causal analysis approaches in ingenuity pathway analysis. Bioinformatics. 2014;30: 523–530. doi:10.1093/bioinformatics/btt703
133. R Core Team. R: A language and environment for statistical computing. R Foundation for Statistical Computing, Vienna, Austria. 2002. Available: https://www.r-project.org/.
134. Fox J. An R Companion to Applied Regression. Third. Sage, Thousand Oaks CA; 2019. Available: https://socialsciences.mcmaster.ca/jfox/Books/Companion/
135. Hothorn T, Bretz F, Westfall P. Simultaneous inference in general parametric models. Biometrical Journal. Biom J; 2008. pp. 346–363. doi:10.1002/bimj.200810425
136. Wickham H. ggplot2 - Elegant Graphics for Data Analysis. Springer; 2016. Available: https://www.springer.com/de/book/9780387981413

bioRxiv preprint doi: https://doi.org/10.1101/2021.06.04.447058; this version posted June 4, 2021. The copyright holder for this preprint (which was not certified by peer review) is the author/funder, who has granted bioRxiv a license to display the preprint in perpetuity. It is made available under a CC-BY 4.0 International license.

Supporting Tables

Table S1. Quantitative RT-PCR analysis of *Tti2* mRNA expression in BN and SHR rats.

Tissue	ΔΔCT (SHR – BN)	*t*	df	*p*-value
Adrenal gland	-0.39 ± 0.13	1.84	9	0.099
Perirenal fat	1.15 ± 0.13	-4.83	8	0.0013
Hippocampus	-0.88 ± 0.1	3.5	8	0.0081
Kidney	-1.14 ± 0.12	5.31	8	0.00072
Liver	-0.85 ± 0.08	2.77	9	0.022
Soleus muscle	-1.49 ± 0.15	7.34	8	8.10E-05
Pancreas	-1.15 ± 0.11	2.49	8	0.037

Expression values were normalised to the mean expression of *Tti2* in BN. Note that lower cycle of threshold (ΔΔCT) values indicate higher relative expression of a gene. Data is shown as means ± standard error of the mean; *t*, Student's *t*-test statistic; df, degrees of freedom.

Table S2. Non-synonymous amino acid substitutions in the SHR *Tti2* coding sequence.

Position	Conservation Score	Reference	SHR	Reference Amino Acid	Variant Amino Acid	Amino Acid Coordinate	Polyphen Prediction	SIFT Prediction
64399852	0.909	T	G	E	D	247	benign	0.15
64401758	0.277	C	T	A	T	205	benign	0.71
64401779	0.567	T	C	K	E	198	benign	1
64402213	0.005	C	T	R	K	53	benign	0.9
64402331	0.001	A	G	C	R	14	benign	0.2
64402360	0	C	T	G	D	4	benign	1

Genomic sequence of SHR rats between positions 62.1 and 66.3 Mb on chromosome 16, which cover neurogenesis-glucose QTL, was scanned for non-synonymous amino-acid substitutions compared to reference genome using Variant Visualiser in Rat Genome Database. Within this interval, missense mutations were present only in the *Tti2* gene.

bioRxiv preprint doi: https://doi.org/10.1101/2021.06.04.447058; this version posted June 4, 2021. The copyright holder for this preprint (which was not certified by peer review) is the author/funder, who has granted bioRxiv a license to display the preprint in perpetuity. It is made available under a CC-BY 4.0 International license.

Conservation score ranges from 1 (highly conserved) to 0 (not conserved). SIFT score ranges from 0 (damaging) to 1 (non-damaging). Positions are according to Rnor_5.0 genome assembly.

Table S3. RNAseq confirmed reduction of *Tti2* mRNA expression in SHR-*Tti2*$^{+/-}$ rats compared to wild type SHR littermates.

Tissue	beta	se	*p* value	*q* value
Hippocampus	-0.54	0.07	1.40E-15	2.8E-11
Liver	-0.53	0.08	7.7E-11	1.8E-07
Fat	-0.46	0.07	1.7E-11	3.5E-07
Muscle	-0.63	0.06	3.70E-22	6.7E-18

bioRxiv preprint doi: https://doi.org/10.1101/2021.06.04.447058; this version posted June 4, 2021. The copyright holder for this preprint (which was not certified by peer review) is the author/funder, who has granted bioRxiv a license to display the preprint in perpetuity. It is made available under a CC-BY 4.0 International license.

Supporting Figure Captions

Fig. S1. Metabolic phenotyping of three-months old heterozygous SHR-*Tti2*$^{+/-}$ rats and wild type SHR- *Tti2*$^{+/+}$ littermates (denoted as SHR).

Details of statistical analysis are in Table 2. Abbreviations: BAT, brown adipose tissue; GSH, glutathione; HDL, high-density lipoprotein; TG, triglycerides.

Fig. S2. Top canonical pathways enriched among differentially expressed genes between SHR-*Tti2*$^{+/-}$ rats and wild type SHR littermates.

Analysis was performed with Ingenuity pathway analysis (IPA), which, in addition to calculating enrichment, predicts activation (positive Z-score, red) or inhibition (negative Z-score, blue) of molecular pathways from the direction and magnitude of expression changes using curated database. Grey bars depict enriched pathways for which activation status could not be predicted. Vertical green dashed line indicates *p* value threshold of 0.05.

Fig. S3. Predicted regulator networks effects involved in glucose homeostasis in livers of SHR-*Tti2*$^{+/-}$ rats

Differentially expressed genes in livers of SHR-*Tti2*$^{+/-}$ rats and wild type SHR littermates were analysed using IPA. Up- (magenta) and downregulated genes (green; middle tier) connect the potential upstream regulators (upper tier) to downstream outcomes (bottom tier). Edges represent relationships derived from curated databases.

Fig. S4. Frequencies of single- and multi-tissue human *TTI2* eQTL.

821 genomic variants underlying 2177 eQTL (p < 1e-4) extracted from eQTL EBI catalogue (https://www.ebi.ac.uk/eqtl/) were clustered according to the number of distinct tissues or cell types in which eQTL were detected. Multiple eQTL from different data sets derived from the same cell or tissue type were scored as a single-tissue eQTL.

bioRxiv preprint doi: https://doi.org/10.1101/2021.06.04.447058; this version posted June 4, 2021. The copyright holder for this preprint (which was not certified by peer review) is the author/funder, who has granted bioRxiv a license to display the preprint in perpetuity. It is made available under aCC-BY 4.0 International license.

Supporting Information Files

File S1. Ingenuity canonical pathways.

IPA canonical pathways enriched in differentially expressed genes in SHR-*Tti2*$^{+/-}$ vs. wild type SHR rats in the hippocampus, liver, muscle and perirenal adipose tissue.

File S2. Ingenuity upstream regulators.

Affected upstream regulators predicted by IPA from differentially expressed genes in SHR-*Tti2*$^{+/-}$ vs. wild type SHR rats in the hippocampus, liver, muscle and perirenal adipose tissue. Activation Z-score sis deduced from the direction and magnitude of the gene expression changes.

File S3. Ingenuity downstream functions and diseases.

Functions enriched among differentially expressed genes in SHR-*Tti2*$^{+/-}$ vs. wild type SHR rats in the hippocampus, liver, muscle and perirenal adipose tissue. IPA deduces the activation Z-scores from the direction and magnitude of the gene expression changes.

File S4. Human *TTI2* eQTL.

Human eQTL catalogue (https://www.ebi.ac.uk/eqtl/) was queried for variants associated with changes in the *TTI2* mRNA expression. Significant eQTL were defined by p value < 1e-4.

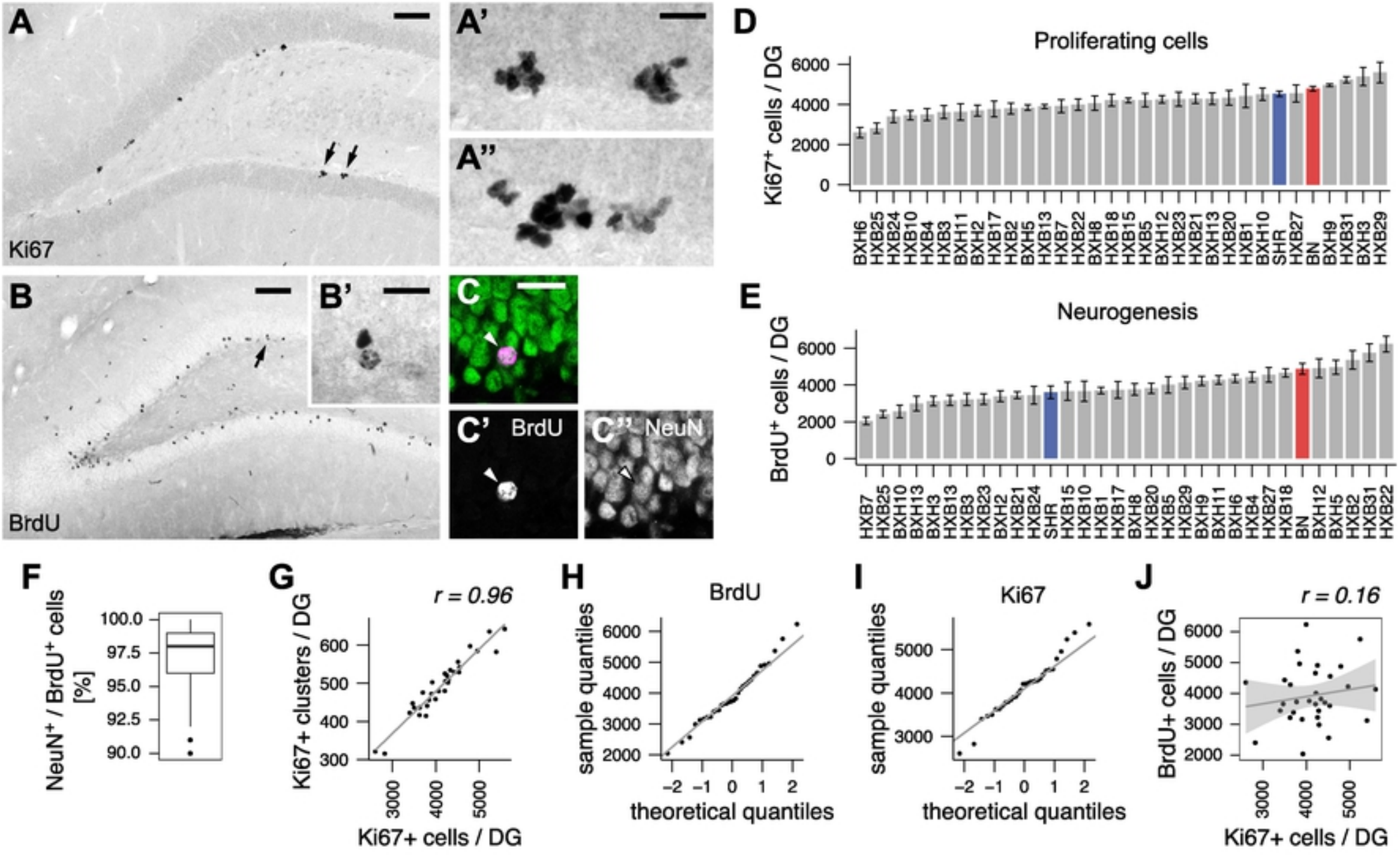
A
A'
A''
Ki67
B
B'
C
C'
BrdU
C''
NeuN
BrdU
D
Proliferating cells
Ki67⁺ cells / DG
6000
4000
2000
0
BXH6 HXB25 HXB24 HXB10 HXB4 HXB3 BXH11 BXH2 HXB17 HXB2 HXB5 HXB13 HXB7 HXB22 BXH8 HXB18 HXB15 HXB5 BXH12 HXB23 HXB21 BXH13 HXB20 HXB1 BXH10 SHR HXB27 BN BXH9 HXB31 BXH3 HXB29
E
Neurogenesis
BrdU⁺ cells / DG
6000
4000
2000
0
HXB7 HXB25 BXH10 BXH13 BXH3 HXB13 HXB3 HXB23 BXH2 HXB21 HXB24 SHR HXB15 HXB10 HXB1 HXB17 BXH8 HXB20 HXB5 HXB29 BXH9 BXH11 BXH6 HXB4 HXB27 HXB18 BN BXH12 BXH5 HXB2 HXB31 HXB22
F
NeuN⁺ / BrdU⁺ cells [%]
100.0
97.5
95.0
92.5
90.0
G
r = 0.96
Ki67+ clusters / DG
600
500
400
300
3000
4000
5000
Ki67+ cells / DG
H
BrdU
sample quantiles
6000
5000
4000
3000
2000
−2 −1 0 1 2
theoretical quantiles
I
Ki67
sample quantiles
5000
4000
3000
−2 −1 0 1 2
theoretical quantiles
J
r = 0.16
BrdU+ cells / DG
6000
5000
4000
3000
2000
3000
4000
5000
Ki67+ cells / DG

Figure 1

bioRxiv preprint doi: https://doi.org/10.1101/2021.06.04.447058; this version posted June 4, 2021. The copyright holder for this preprint (which was not certified by peer review) is the author/funder, who has granted bioRxiv a license to display the preprint in perpetuity. It is made available under aCC-BY 4.0 International license.

Figure 2

bioRxiv preprint doi: https://doi.org/10.1101/2021.06.04.447058; this version posted June 4, 2021. The copyright holder for this preprint (which was not certified by peer review) is the author/funder, who has granted bioRxiv a license to display the preprint in perpetuity. It is made available under aCC-BY 4.0 International license.

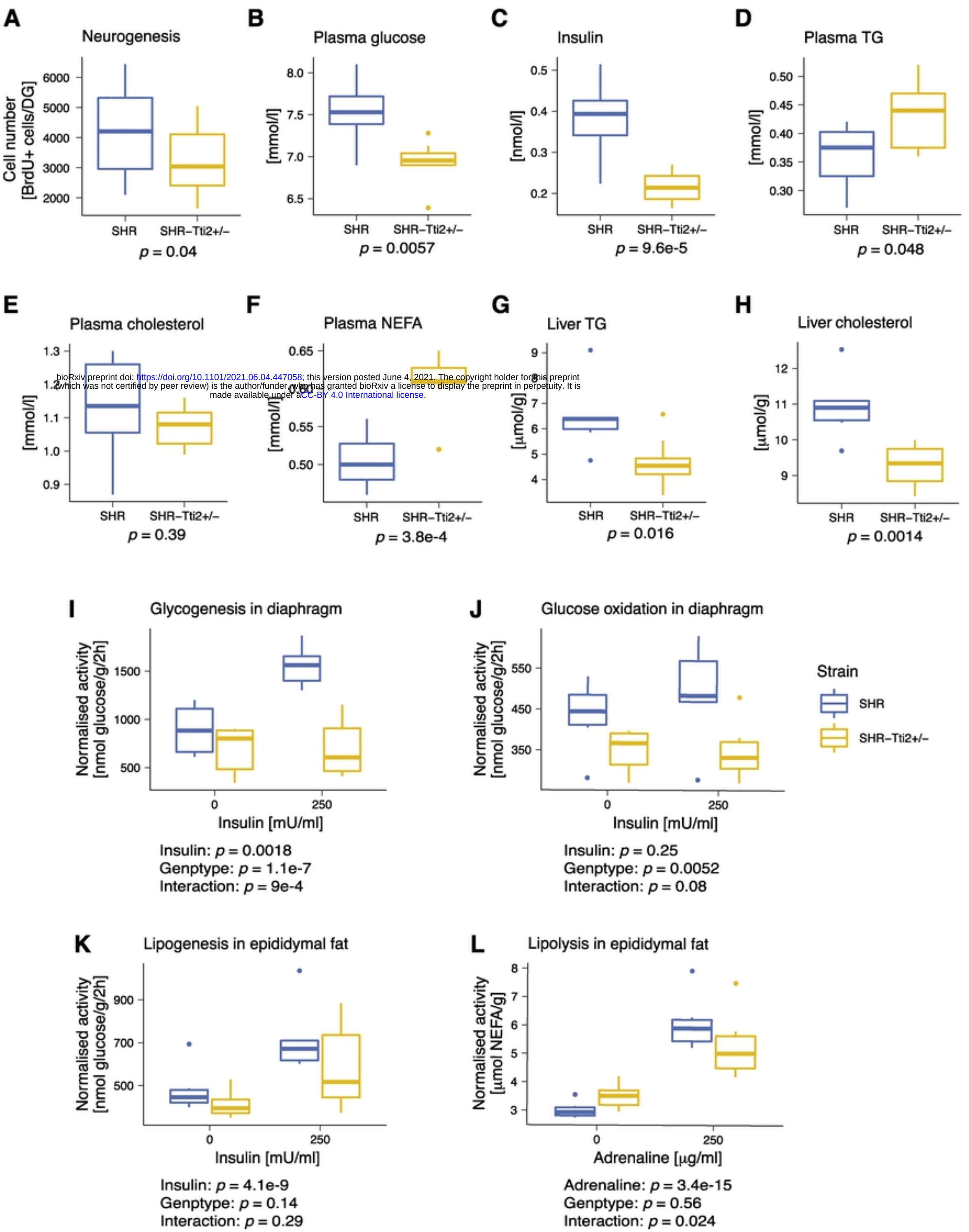

Figure 3

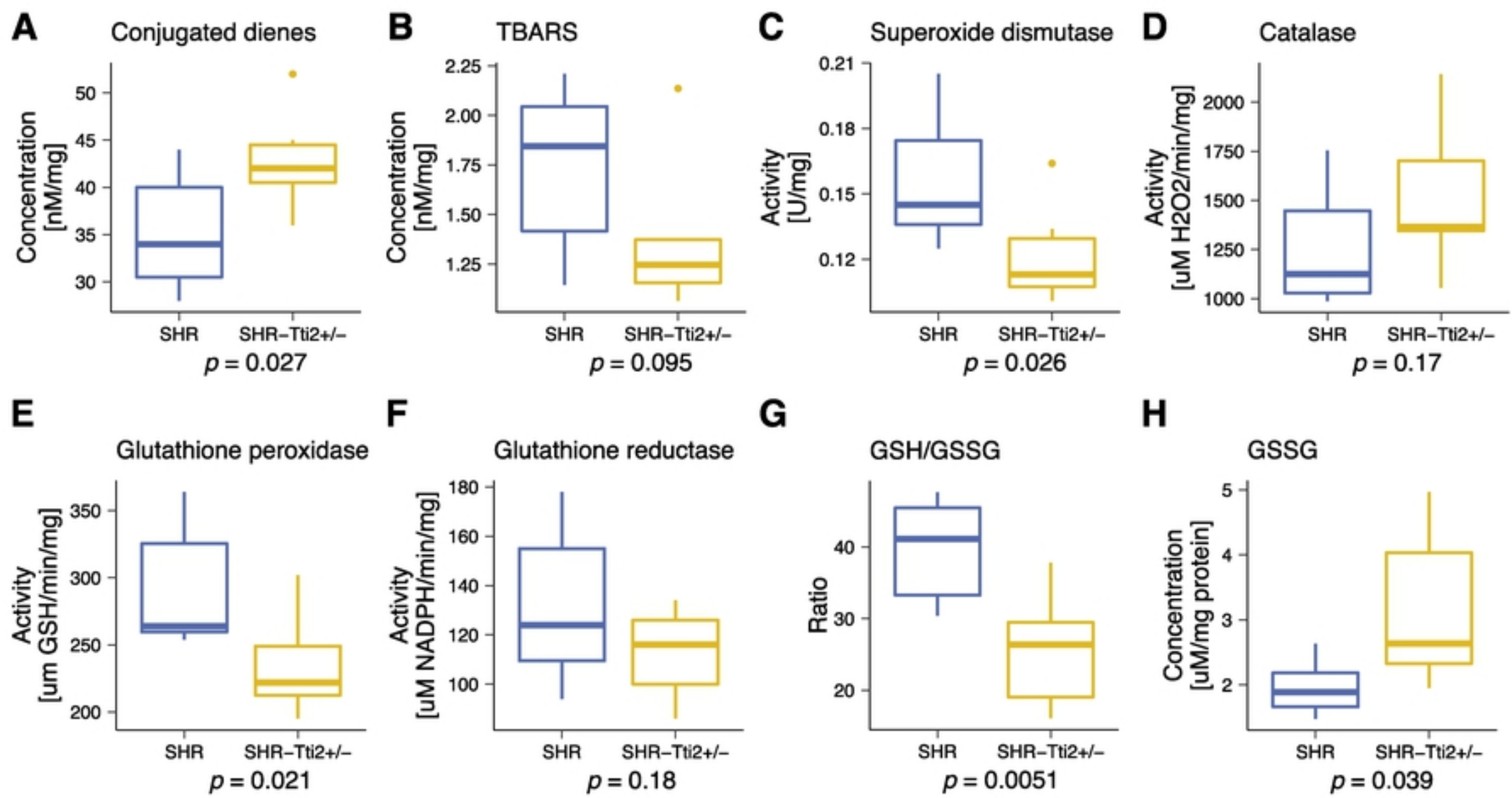
A
Conjugated dienes
Concentration [nM/mg]
50
45
40
35
30
SHR
SHR–Tti2+/–
p = 0.027
B
TBARS
Concentration [nM/mg]
2.25
2.00
1.75
1.50
1.25
SHR
SHR–Tti2+/–
p = 0.095
C
Superoxide dismutase
Activity [U/mg]
0.21
0.18
0.15
0.12
SHR
SHR–Tti2+/–
p = 0.026
D
Catalase
Activity [uM H2O2/min/mg]
2000
1750
1500
1250
1000
SHR
SHR–Tti2+/–
p = 0.17
E
Glutathione peroxidase
Activity [um GSH/min/mg]
350
300
250
200
SHR
SHR–Tti2+/–
p = 0.021
F
Glutathione reductase
Activity [uM NADPH/min/mg]
180
160
140
120
100
SHR
SHR–Tti2+/–
p = 0.18
G
GSH/GSSG
Ratio
40
30
20
SHR
SHR–Tti2+/–
p = 0.0051
H
GSSG
Concentration [uM/mg protein]
5
4
3
2
SHR
SHR–Tti2+/–
p = 0.039

Figure 4

bioRxiv preprint doi: https://doi.org/10.1101/2021.06.04.447058; this version posted June 4, 2021. The copyright holder for this preprint (which was not certified by peer review) is the author/funder, who has granted bioRxiv a license to display the preprint in perpetuity. It is made available under aCC-BY 4.0 International license.

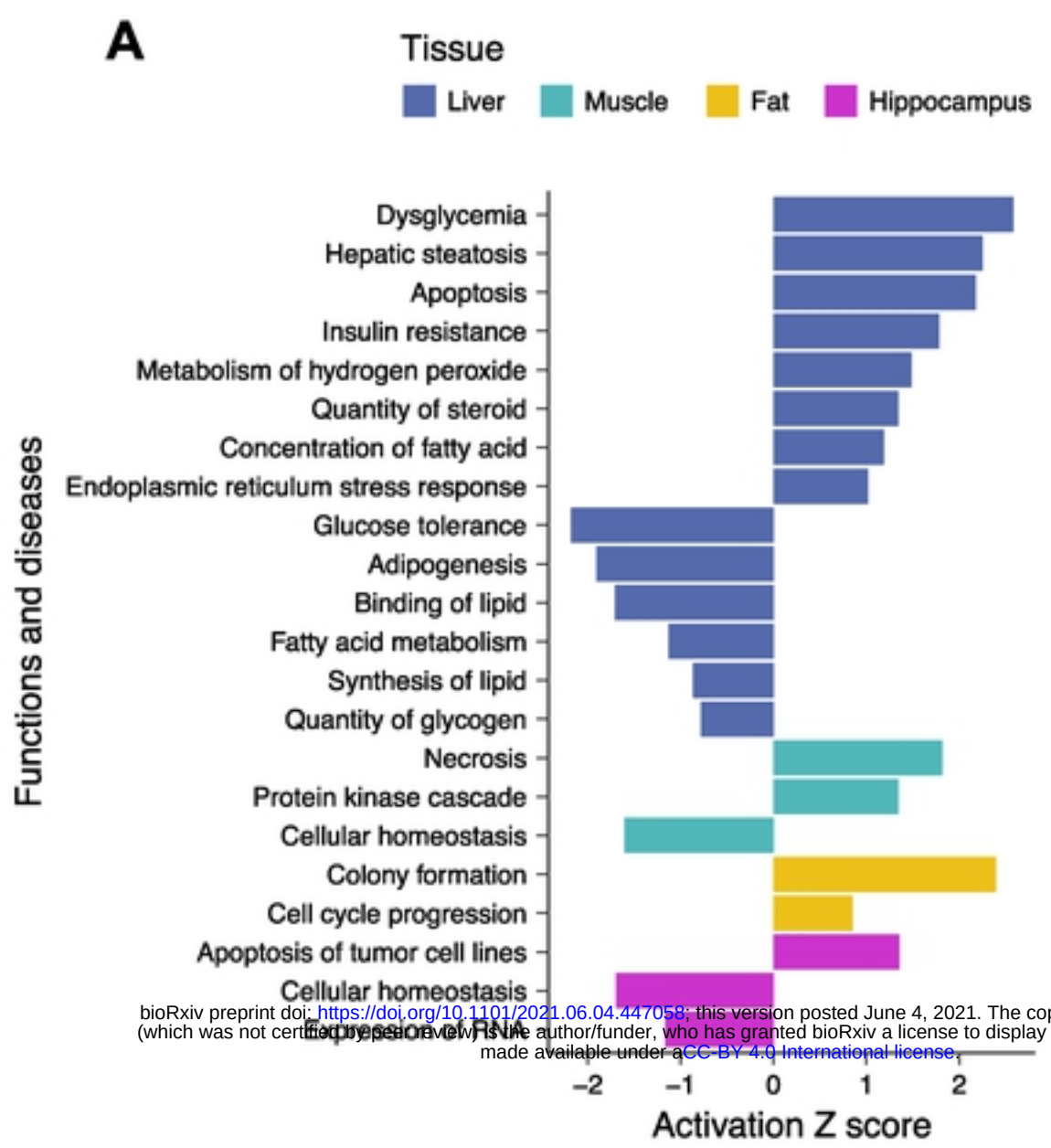

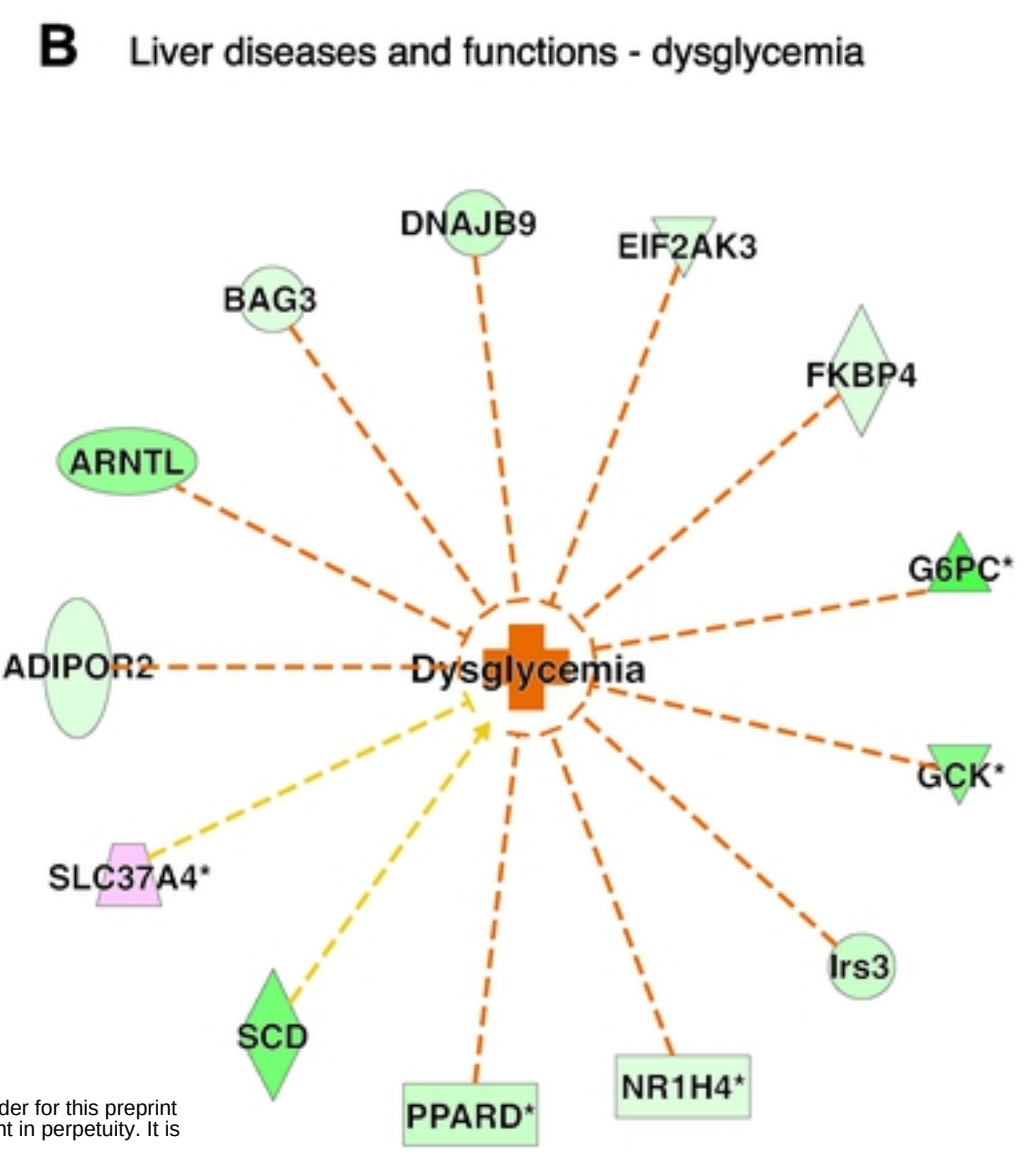

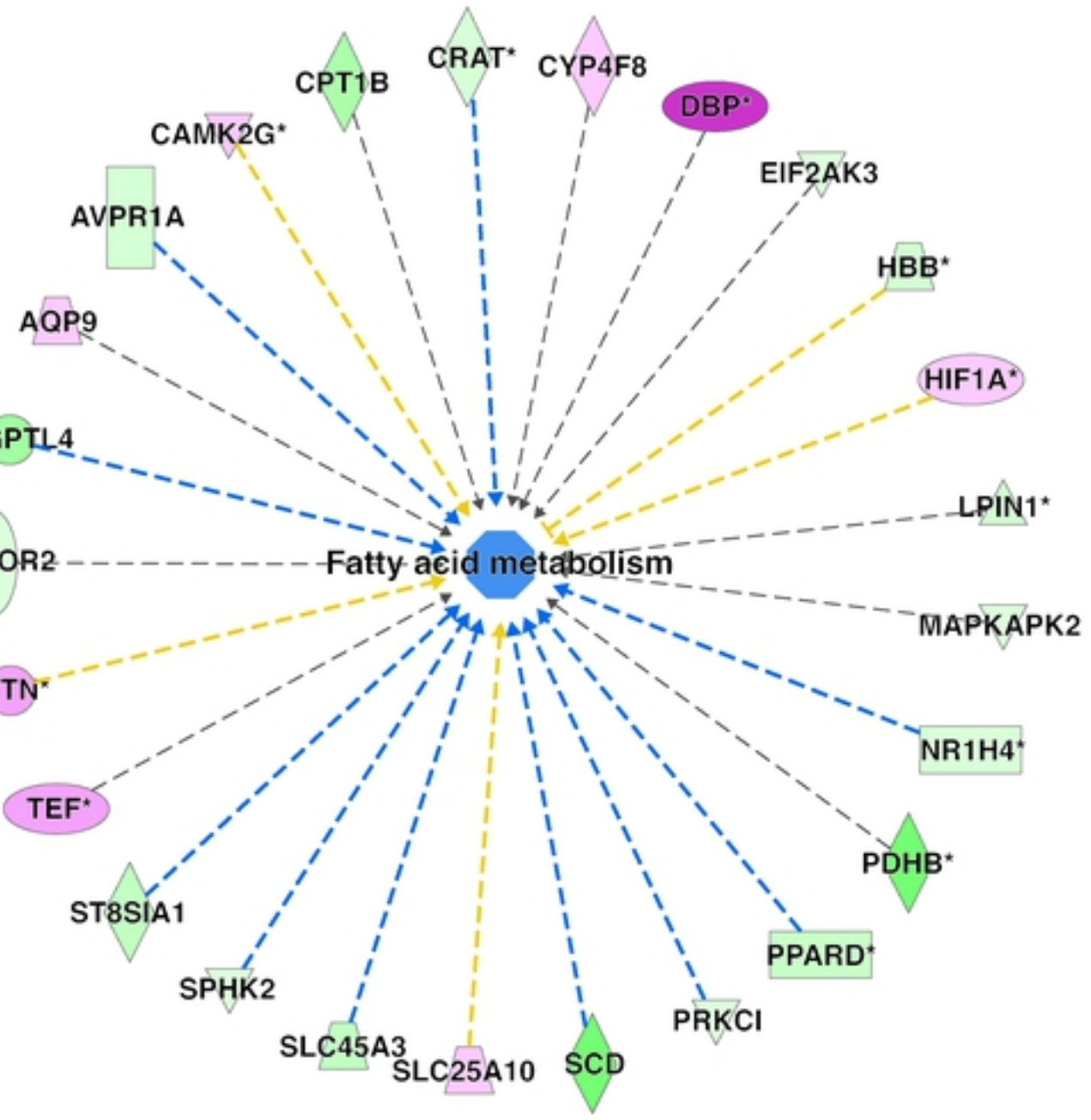

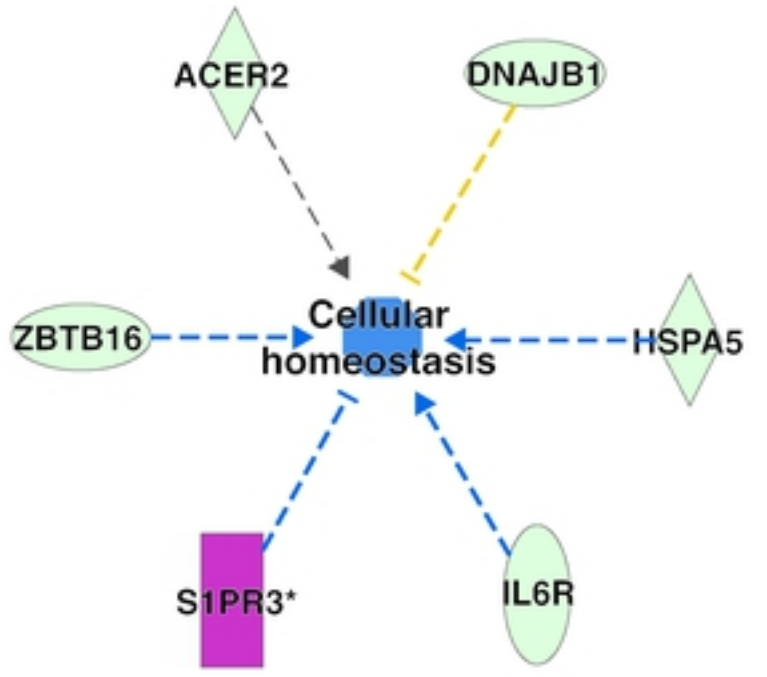

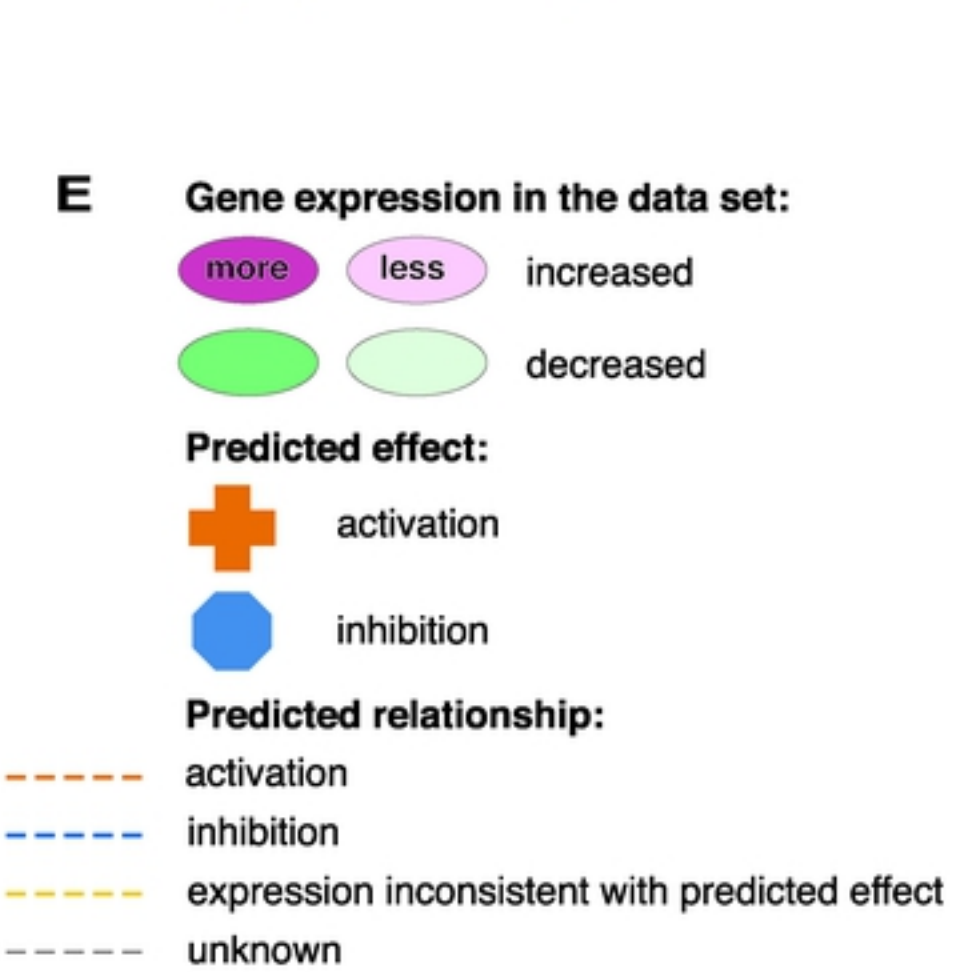

Figure 5